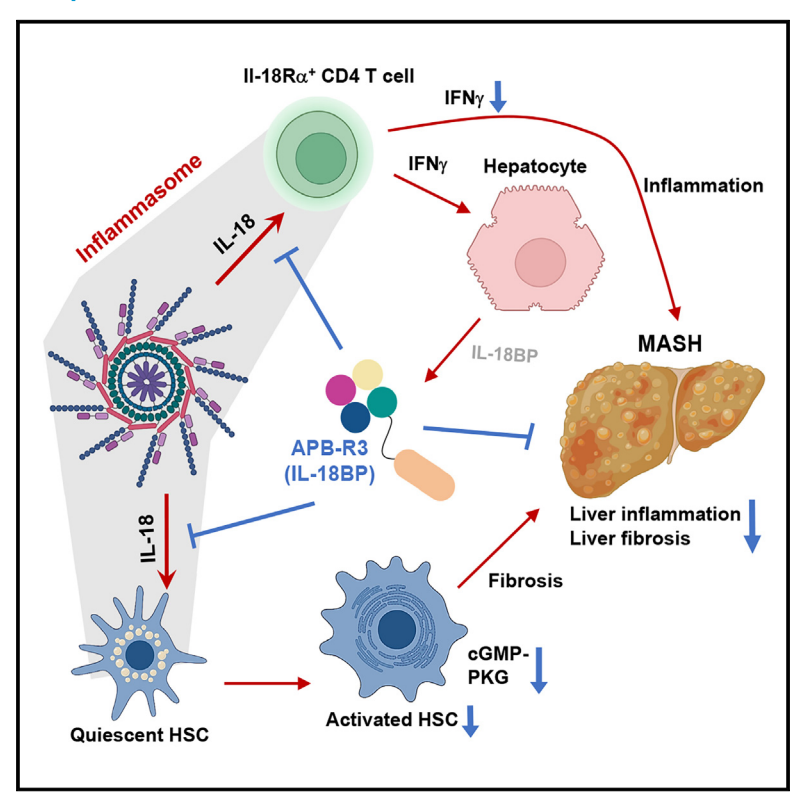
Treatment of IL-18-binding protein biologics suppresses fibrotic progression in metabolic dysfunction-associated steatohepatitis

Graphical abstract



Authors

Dong-Hyun Kim, Gona Choi, Eun-Bi Song, ..., Seung Goo Kang, Sang-Hoon Cha, Yong-Hyun Han

Correspondence

sgkang@kangwon.ac.kr (S.G.K.), chash@aprilbio.com (S.-H.C.), yhhan1015@kangwon.ac.kr (Y.-H.H.)

In brief

Kim et al. discover that IL-18BP is a key modulator of hepatic inflammation and fibrosis in MASH. The engineered longacting IL-18BP biologics, APB-R3, displays anti-inflammatory and -fibrosis effect via regulation of IFN signaling and HSC activation. Treatment of IL-18BP biologics is an attractive strategy to cure MASH injuries.

Highlights

- The amounts of free IL-18 are increased in MASH despite the enhancement of IL-18BP protein
- Overwhelmed IL-18 signaling exacerbates hepatic inflammation and fibrosis
- The engineered IL-18BP biologics inhibits MASH via blockade of IFN signaling
- IL-18BP biologics suppresses hepatic fibrosis in MASH through HSC inactivation







Article

Treatment of IL-18-binding protein biologics suppresses fibrotic progression in metabolic dysfunction-associated steatohepatitis

Dong-Hyun Kim,^{1,9} Gona Choi,^{1,9} Eun-Bi Song,^{1,9} Hanna Lee,^{1,2,9} Jaehui Kim,^{3,4,9} Young-Saeng Jang,^{3,4} JinJoo Park,⁵ Susan Chi,⁵ Jaekyu Han,⁵ Sun-Mi Kim,⁵ Dongyoon Kim,⁶ Soo Han Bae,⁷ Hye Won Lee,⁸ Jun Yong Park,⁸ Seung Goo Kang,^{3,4,*} Sang-Hoon Cha,^{4,5,*} and Yong-Hyun Han^{1,2,10,*}

SUMMARY

Metabolic dysfunction-associated steatohepatitis (MASH) is a chronic liver disease characterized by inflammation and fibrosis, with enhanced interleukin-18 (IL-18) signaling. IL-18-binding protein (IL-18BP) neutralizes IL-18, but its therapeutic potential in MASH is unclear. We find elevated IL-18BP and IL-18 levels in patients with MASH and mice, with free IL-18 correlating with disease severity. IL-18 stimulates interferongamma (IFN γ) production in CD4 T cells, increasing hepatic IL-18BP. IL-18BP-deficient mice show worsened liver inflammation and fibrosis. We develop a human IL-18BP biologics (APB-R3) and inject it to mice to evaluate its pharmacologic efficacy. APB-R3 significantly improves MASH in reducing fibrosis and inflammation and inhibits hepatic stellate cell activation via the cGMP pathway. This study proposes that abrogation of IL-18 signaling by boosting IL-18BP can strongly inhibit the development of MASH-induced fibrosis, and our engineered IL-18BP biologics can become a promising therapeutic candidate for curing MASH.

INTRODUCTION

Metabolic dysfunction-associated steatohepatitis (MASH) is a chronic liver disease featured by a broad spectrum of metabolic dysfunction-associated fatty liver disease (MAFLD) ranging from simple fatty liver to chronic liver inflammation and remarkable fibrotic formation. The prevalence of MASH is expected to gradually increase by 63% from 2015 to 2030 due to the high occurrence of adult obesity and increases in aging diseases.² In particular, MASH-induced hepatic fibrosis and cirrhosis can notably influence the mortality rate of patients with MASH by leading to the onset of cardiovascular disease and neuro-cognitive dysfunction.³ Hepatic fibrosis is featured by excessive deposition of extracellular matrix (ECM) and scarring through persistent cell death and inflammation in the liver. 4 Hepatic stellate cells (HSCs) are key players in liver fibrosis progression because activated HSCs highly express proteins associated with ECM production and scar formation, leading to the development toward myofibroblast. Extracellular mediators such as transforming

growth factor β (TGF- β) released from inflammatory cells can promote imbalanced HSC activation. Interestingly, inflammasome activation can induce fibrotic phenotypes of HSCs, thereby triggering hepatic fibrosis in a murine model. Emerging concept of inactivating HSCs to inhibit fibrotic progression has been focused on curing hepatic fibrosis in MASH. However, an approved therapeutic strategy to disturb HSC activation to relieve MASH and fibrosis is currently unavailable.

Interleukin-18 (IL-18) is a pro-inflammatory cytokine that plays a crucial role in the immune system by regulating immune response to infection and inflammation. IL-18 is secreted by activation of NOD-like receptor family, pyrin domain-containing 3 (NLRP3) inflammasome. IL-18 can stimulate natural killer (NK) cells and T lymphocytes to produce type 1 cytokines such as interferon-gamma (IFN γ). While IL-18 is essential for mounting an effective immune response, uncontrolled action and production of IL-18 can lead to harmful catastrophe by causing chronic inflammation and tissue damage. Therefore, our body employs a natural neutralizer for IL-18 known as IL-18-binding protein



¹Laboratory of Pathology and Physiology, College of Pharmacy, Kangwon National University, Chuncheon 24341, South Korea

²Multidimensional Genomics Research Center, Kangwon National University, Chuncheon 24341, South Korea

³Division of Biomedical Convergence, College of Biomedical Science, Kangwon National University, Chuncheon 24341, South Korea

⁴Institute of Bioscience and Biotechnology, College of Biomedical Science, Kangwon National University, Chuncheon 24341, South Korea

⁵AprilBio Co., Ltd, Biomedical Science Building, Kangwon National University, Chuncheon 24341, South Korea

⁶Department of Bioengineering, University of Pennsylvania, Philadelphia, PA 19104, USA

⁷Severance Biomedical Science Institute, Graduate School of Medical Science, Brain Korea 21 Project, Yonsei University College of Medicine, Seoul 03722, South Korea

⁸Division of Gastroenterology, Department of Internal Medicine, Yonsei University College of Medicine, Seoul 03722, South Korea ⁹These authors contributed equally

¹⁰Lead contact

^{*}Correspondence: sgkang@kangwon.ac.kr (S.G.K.), chash@aprilbio.com (S.-H.C.), yhhan1015@kangwon.ac.kr (Y.-H.H.) https://doi.org/10.1016/j.xcrm.2025.102047



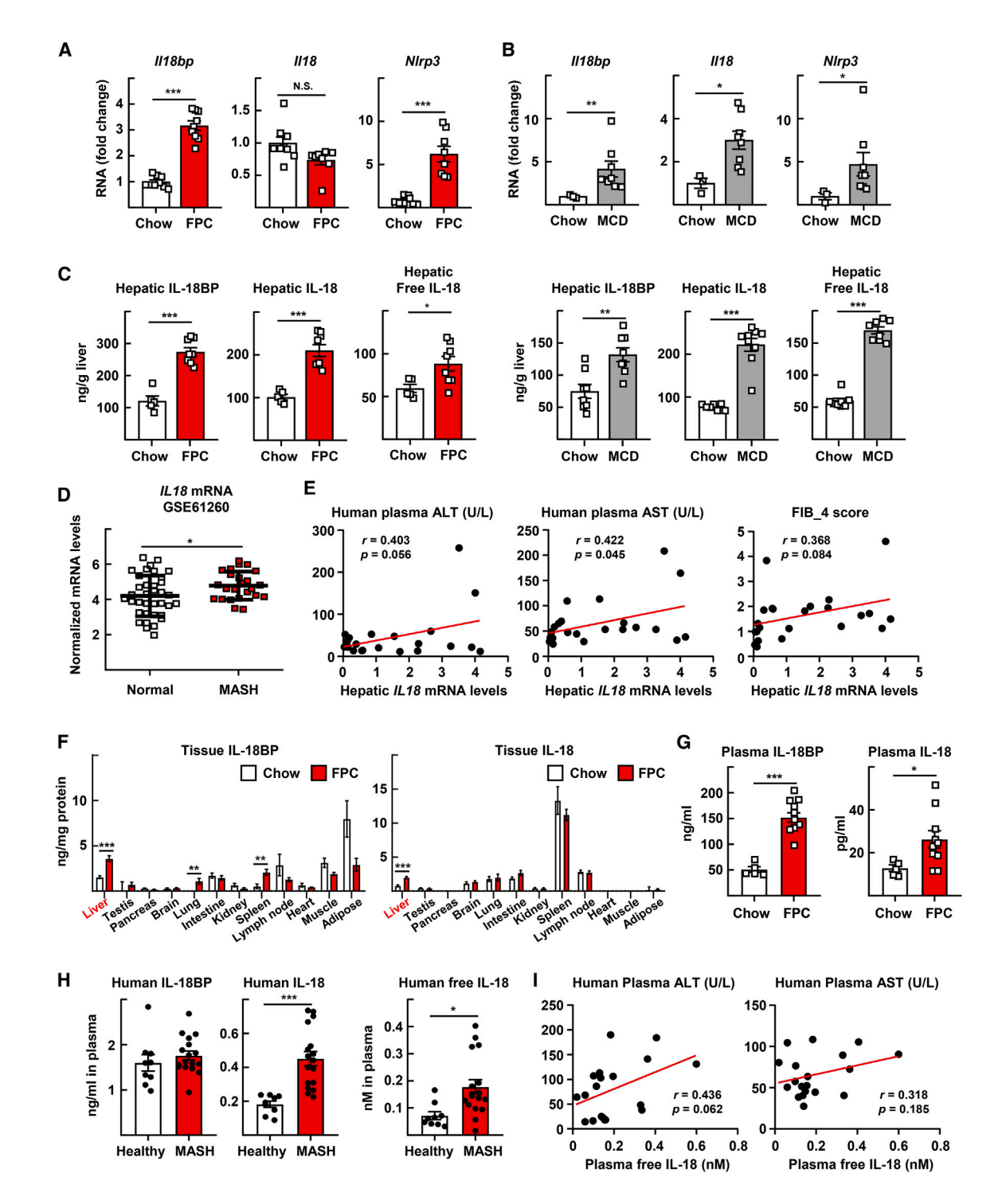


Figure 1. Hepatic IL-18BP and IL-18 are elevated under MASH condition

Male C57BL/6J mice were fed with FPC diet for 16 weeks or with MCD diet for 6 weeks.

(A) Measurement of *II18bp*, *II18*, and *NIrp3* mRNA levels in the livers obtained from chow or FPC diet-fed mice by quantitative reverse-transcription PCR (qRT-PCR) (n = 8 or 9)

- (B) Measurement of II18bp, II18, and NIrp3 mRNA levels in the livers obtained from chow or MCD diet-fed mice by qRT-PCR (n = 3 or 8).
- (C) ELISA assay was conducted to measure hepatic amounts of IL-18BP, IL-18, and free IL-18 in FPC (left, n=5 or 8) or MCD (right, n=8) diet-fed mice.
- (D) Gene expression analysis was conducted using public datasets obtained from GEO site at the NCBI (GSE61260). Hepatic mRNA levels of IL18 were analyzed. The data processed as quantile normalized intensity value (n = 38 for normal; n = 24 for MASH).

(legend continued on next page)

Article



(IL-18BP) which is a soluble protein that can directly bind to IL-18, thereby blocking its interaction with IL-18 receptors. IL-18BP can prevent pro-inflammatory activation of IL-18 and help maintain immune homeostasis. Impaired balance of IL-18 and IL-18BP has been implicated in various disorders, including autoimmune diseases, cancers, and infectious diseases.

Constitutively activated NLRP3 can promote the production of IL-1β and IL-18, resulting in spontaneous induction of hepatic inflammation and fibrosis in mice. Indeed, patients with MASH exhibit amplified activities of NLRP3 and caspase-1 in their livers. 10 Blockade of NLRP3 inflammasome after treatment with MCC950, a selective inhibitor of NLRP3 inflammasome, can effectively attenuate liver inflammation and scarring formation in MASH mouse models. 11 Interestingly, disturbance of IL-1β by an IL-1 receptor antagonist could not rescue the degree of fibrosis, indicating that other NLRP3-dependent players contribute to fibrotic activation.9 Recently, it has been found that IL-18 can directly drive HSC activation in hyperactivated NLRP3 models, indicating the role of IL-18 in the development of hepatic fibrosis. 12 In addition, enhanced IL-18 signaling can exacerbate liver inflammation through NK and T cell-mediated IFN_γ productions. ¹³ Plasma concentrations of IL-18 are elevated in patients with chronic liver cirrhosis and correlated with disease severity. 14 Thus, pharmacological approaches that can inhibit IL-18 signaling might provide a promising opportunity to ameliorate MASH-driven inflammation and fibrosis.

In severe condition of chronic liver diseases, amounts of plasma IL-18BP are increased. However, elevated IL-18BP levels are insufficient to prevent disease progression.¹⁴ Exogenous injection of IL-18BP can ameliorate endotoxin-induced liver damages. 15 Therefore, we examined the therapeutic potential of IL-18BP to cure liver inflammation and fibrosis in multiple MASH models. Herein, we found that free IL-18 levels were elevated under MASH conditions even if the production of IL-18BP was increased. Systemic loss of IL-18BP largely exacerbated liver inflammation and fibrosis in a mouse model of MASH. We further employed our engineered IL-18BP biologics (APB-R3), which showed a long serum half-life in rodent and monkey. Here, we provide clear evidence for the therapeutic potency of IL-18BP biologics to ameliorate hepatic fibrosis in multiple MASH models. Our results suggest a novel approach of combining IL-18BP biologics with anti-steatotic agents to relieve MASH development.

RESULTS

Hepatic free IL-18 is elevated in MASH condition despite increased expression of IL-18BP

To analyze hepatic IL-18 signaling under an experimental MASH condition, we employed a fructose, palmitate, and cholesterol

and trans-fat (FPC) and a methionine choline-deficient (MCD) diet to induce steatohepatitis, fibrosis, and inflammasome activation in C57BL/6J mice. 11,16 It was found that mRNA levels of II18bp in the liver were induced by feeding with FPC and MCD diets (Figures 1A and 1B). Consistently, hepatic amounts of IL-18BP proteins were increased under MASH conditions (Figure 1C). Transcriptional levels of the I/18 gene were not upregulated in the livers of FPC-fed mice. However, IL-18 protein levels were elevated because NLRP3 was activated following MASH injury (Figures 1A-1C). Ileum-derived IL-18 was also enhanced in MASH condition (Figure S1A). Active free IL-18 levels were still higher in MASH livers, although amounts of IL-18BP protein were augmented, suggesting that elevated levels of IL-18BP were insufficient to completely inhibit IL-18 signaling (Figures 1A-1C). Transcriptional levels of IL-18 receptors (II18r1, II18rap) were also increased in MASH livers (Figure S1B). Analysis of public human NCBI database (GSE61260) showed that transcription levels of hepatic genes associated with IL-18BP and IL-18 pathway were significantly higher in MASH livers than in normal livers (Figures 1D and S1C). Interestingly, hepatic transcription levels of human IL18 showed positive correlations with MASH injury markers such as plasma alanine aminotransferase (ALT)/aspartate aminotransferase (AST) levels and Fibrosis-4 Index (FIB_4) score (Figure 1E). Next, we investigated the amount of IL-18BP and IL-18 in many tissues to check local or systemic effects. Liver was not an organ that expressed IL-18BP and IL-18 the most abundantly compared to other organs, but FPC diet only increased amounts of IL-18BP and IL-18 in the liver, guessing that IL-18 and IL-18BP could locally contribute to liver diseases (Figure 1F). However, increased production of hepatic IL-18BP and IL-18 caused by feeding the FPC diet and a choline-deficient L-amino acid-defined high-fat diet (CDAA-HFD) resulted in elevated plasma concentration of IL-18BP and IL-18 (Figures 1G and S1D). We observed that concentrations of plasma IL-18 were increased in human patients with MASH as well, whereas IL-18BP levels were not significantly higher in patients with MASH compared to a healthy control group (Figure 1H). Therefore, the level of circulating free IL-18 in human was elevated under MASH condition. It exhibited prominent positive correlation with plasma ALT/AST levels, indicating that plasma free IL-18 could be a predictive marker for the progression of catastrophic MASH (Figure 1I). Taken together, these results propose the relevance of increased IL-18BP and activated IL-18 signaling clinically and experimentally in MASH progression.

Augmented IL-18 promotes the release of hepatic IL-18BP via IFN γ production

To further elucidate the relevance of IL-18 and IL-18BP in hepatic inflammation, we performed immunostaining of IL-18BP in FPC and MCD-fed mice. MASH liver tissues exhibited obvious

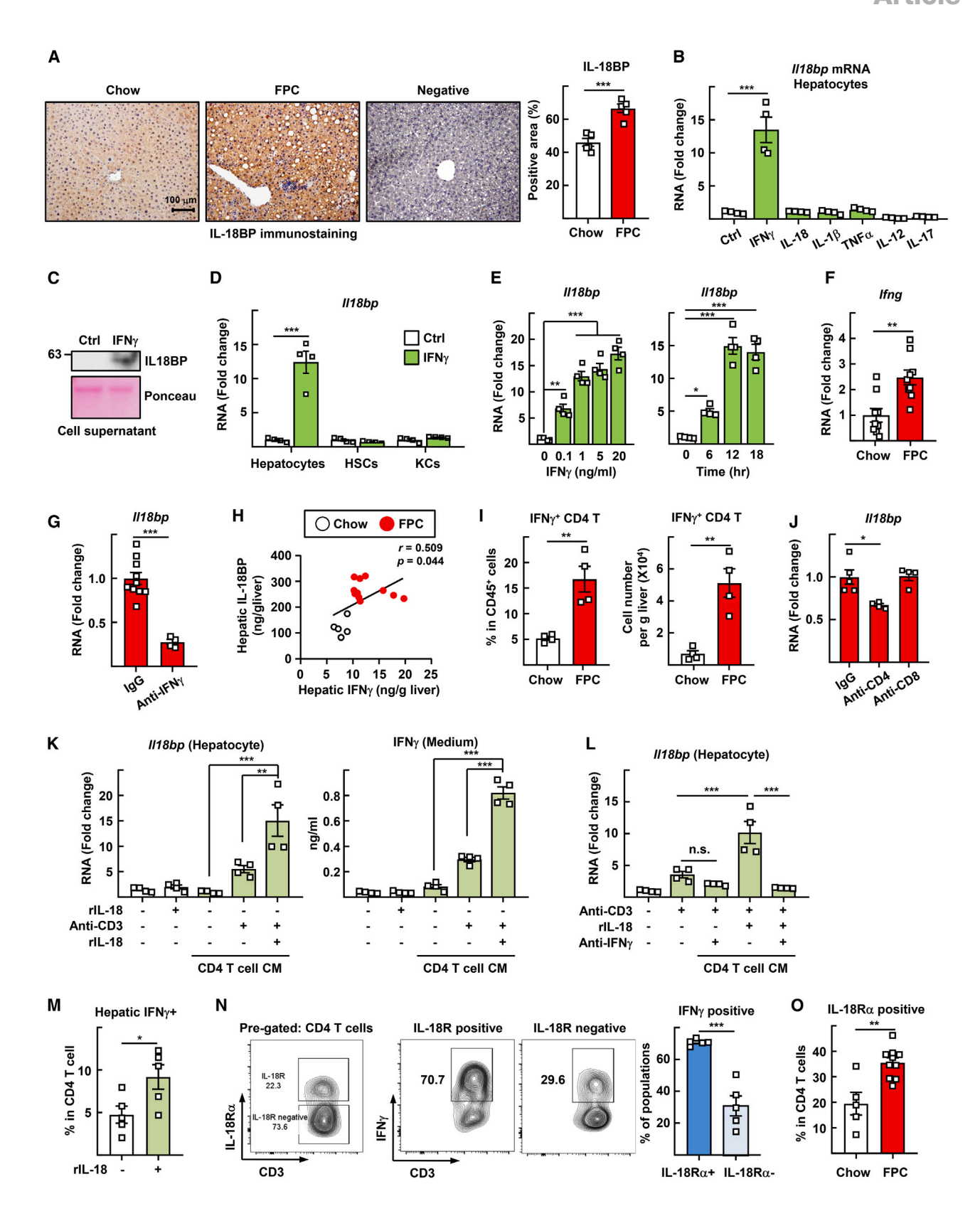
⁽E) Correlation between mRNA levels of hepatic *IL18* and parameters of liver injuries including plasma ALT, AST, and FIB_4 score in the livers of human patients with MASH (n = 23).

⁽F) Tissue expression of IL-18BP and IL-18 in chow or FPC diet-fed mice (n = 4).

⁽G) ELISA assay was conducted to measure plasma concentration of IL-18BP and IL-18 in FPC diet-fed mice (n = 5 or 10).

⁽H) ELISA assay was conducted to measure concentrations of IL-18BP, IL-18, and free IL-18 in plasma of human patients with healthy and MASH (n = 9 or 17). (I) Correlation between plasma free IL-18 and parameters of liver injuries including plasma ALT and AST levels obtained from human patients with MASH (n = 19). *p < 0.05, **p < 0.01, and ***p < 0.001. The data represent mean ± SEM. The data were analyzed by the unpaired two-sided Student's t test for simple comparisons or one-way ANOVA with Tukey's post hoc test for multiple groups.





Article



steatosis and inflammatory foci based on hematoxylin and eosin (H&E) staining of tissue sections (data not shown). Herein, IL-18BP expression levels in liver tissues were significantly enhanced under MASH condition, especially in parenchymal hepatocytes (Figure 2A). To delineate the inducer of IL-18BP in hepatocytes, we stimulated primary hepatocytes with several inflammatory cytokines related to hepatic inflammation. Among them, IFNy markedly induced mRNA expression and secretion of IL-18BP on primary hepatocytes (Figures 2B and 2C). IFNγ only enhanced II18bp mRNA levels in hepatocytes, not in stellate cells and Kupffer cells (Figure 2D). The treatment with IFN γ at 1 ng/mL for 12 h sufficiently induced II18bp mRNA expression (Figure 2E). Indeed, the transcriptional level of Ifng was notably increased (Figure 2F), and the blockade of IFNγ attenuated the expression of II18bp mRNA (Figure 2G) in the livers of MASH mice. Crucially, levels of both IFN_γ and IL-18BP in the livers of MASH mice were elevated, and their positive correlation between these proteins (Figures 2H, S2A, and S2B) suggests that IFN γ is responsible for IL-18BP expression in the livers of two distinct MASH models. To gain further understanding of the IFN- γ -IL-18BP regulatory pathway, we analyzed the number of IFN $\!\gamma\!$ -producing cells, including T cells, NK cells, and ILC1 in the liver of a MASH mouse model. While normal and MASH model mice showed comparable proportion and numbers of CD8 T cells, NK cells, and ILC1 (Figures S2C and S2D), the number of IFN γ^+ CD4 T cells in the FPC and MCD diet-fed group was substantially higher than in the control group fed with a chow diet (Figures 2I and S2B). Furthermore, depletion of CD4 T cells using an anti-CD4 antibody led to a decrease in II18bp expression in the liver, suggesting that CD4 T cells might play a role in requlating the IFNγ-IL-18BP axis in the liver (Figure 2J). IL-18 is a potent stimulant that can effectively increase the production of IFN_γ from CD4 T cells through IL-18 receptor-mediated pathways. Thus, we investigated the function of IL-18 in this regulatory axis. II18bp transcription in hepatocytes was not directly stimulated by IL-18. However, the expression of II18bp in hepatocytes was significantly enhanced by a conditioned medium (CM) of activated CD4 T cells following anti-CD3 treatment in combination with IL-18 (Figure 2K). Furthermore, the expression

level of IFN γ in the CM corresponded to the level of II18bp expression (Figure 2K). Its induction was minimized by the use of an anti-IFNγ-neutralizing antibody (Figure 2L). These findings suggest that CD4 T lymphocytes activated by IL-18 are accountable for the release of IL-18BP from primary hepatocytes by increasing the production of IFN γ . Indeed, CD4 T cells obtained from livers of MASH model mice exhibited a response to IL-18 and produced higher IFNy (Figure 2M). In contrast, CD8 T and NK cells did not respond to IL-18 in terms of IFN γ production (data not shown). In particular, CD4 T cells in the livers of mice with MASH could be grouped as either IL-18R α^+ or IL-18R α^- CD4 T cells. The former group primarily consisted of cells that produced IFN_γ (Figure 2N). Notably, the percentage of IL-18Rα⁺ CD4 T cells was significantly higher in the MASH model of mice than in the control group (Figure 20). Collectively, our findings indicate that elevated IL-18Rα⁺ CD4 T cells, which respond to higher IL-18 levels and directly generate IFNγ via the IL-18-CD4 T-IL-18BP axis, can function as regulators of hepatic inflammation by stimulating the expression of IL-18BP in the MASH model.

Knockout of IL-18BP worsens liver inflammation and fibrosis in MASH models

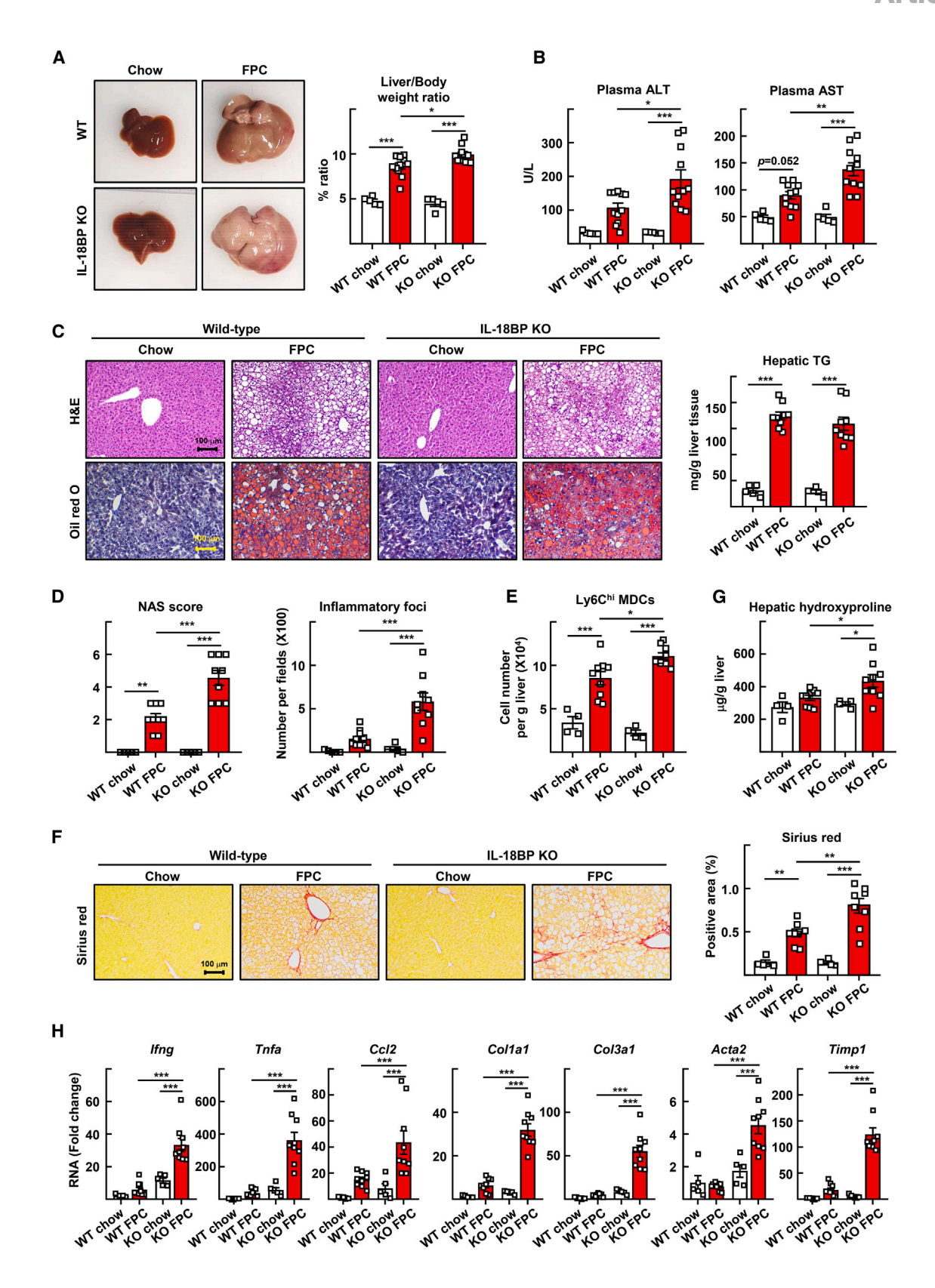
Given that IL-18BP has the potential to act as a modulator of hepatitis, we generated IL-18BP knockout (KO) mice using CRISPR-Cas9 method and investigated the effect of IL-18BP deficiency on MASH progression (Figure S3A). 17 Body weights of mice were not significantly different between wild-type and IL-18BP KO groups after FPC diet feeding (Figure S3B). Compared to FPC-fed WT (WT FPC) mice, FPC-fed IL-18BP KO (KO FPC) mice showed largely increased indicators of MASH symptoms including liver/body weight ratio and plasma ALT/AST levels (Figures 3A and 3B). However, lipid accumulation and hepatic triglyceride (TG) levels did not differ between WT FPC and KO FPC groups of mice, indicating that loss of IL-18BP did not affect hepatic steatosis, although IL-18BP KO mice showed increased transcription levels of genes related with lipid synthesis, transport, and breakdown (Figures 3C, S3C, and S3D). Instead, the nonalcoholic fatty liver disease

Figure 2. Augmented IL-18 leads to release of hepatic IL-18BP via T cell-driven IFN γ production

- (A) Representative images of IL-18BP immunostaining in FPC diet-fed liver sections. Scale bar, 100 µm. Stained area of IL-18BP was measured by ImageJ (n = 5).
- (B) Measurement of II18bp mRNA levels treated with pro-inflammatory cytokines in primary hepatocytes (n = 4).
- (C) Immunoblot for IL-18BP in cell supernatant obtained from IFNγ-treated primary hepatocytes.
- (D) Measurement of II18bp mRNA levels treated with IFN γ in primary hepatocytes, hepatic stellate cells (HSCs), and Kupffer cells (KCs) (n = 4).
- (E) Primary hepatocytes were treated with IFN γ as indicated concentrations (18 h) and time intervals (20 ng/mL), and then II18bp mRNA levels were measured (n = 4).
- (F) Measurement of Ifng mRNA levels in the livers obtained from chow or FPC diet-fed mice (n = 9).
- (G) Neutralizing antibodies against IFN γ were injected in FPC diet-fed mice. Hepatic II18bp mRNA levels were measured (n = 10 or 4).
- (H) Correlation between hepatic amounts of IL-18BP and IFN γ in livers obtained from chow and FPC diet-fed mice (n = 15).
- (I) The percentages and numbers of IFN_Y-positive CD4 T cells in the FPC diet-fed livers were analyzed by flow cytometry (n = 4).
- (J) Neutralizing antibodies against CD4 or CD8 were injected in FPC diet-fed mice. Hepatic #18bp mRNA levels were measured (n = 5 or 4).
- (K) Primary hepatocytes were incubated with conditioned medium (CM) from the culture of anti-CD3 or recombinant IL-18 (rIL-18)-pretreated CD4 T cells for 18 h. Measurement of *II18bp* mRNA levels was performed by qRT-PCR (left, *n* = 4). The concentrations of IFN_Y (right) in hepatocytes medium were measured (right, *n* = 4).

 (L) Primary hepatocytes were incubated with CM from the culture of anti-CD3 or rIL-18-pretreated CD4 T cells for 18 h with anti-IFN_Y anti-hody. Measurement of
- (L) Primary hepatocytes were incubated with CM from the culture of anti-CD3 or rIL-18-pretreated CD4 T cells for 18 h with anti-IFN γ antibody. Measurement of II18bp mRNA levels was performed by qRT-PCR (n=4).
- (M) Isolated CD4 T cells from MASH-induced liver were treated with rIL-18 ex vivo. The percentage of IFNγ-positive cells was analyzed (n = 5).
- (N) The hepatic percentage of IFN γ -positive cells within IL-18R α ⁺ or IL-18R α ⁻ CD4 T cells was analyzed by flow cytometry (n = 5).
- (0) The percentage of IL-18Rα-positive cells within CD4 T cells obtained from livers of chow and FPC diet-fed mice was analyzed (n = 5 or 10).
- *p < 0.05, **p < 0.01, and ***p < 0.001. The data represent mean \pm SEM. The data were analyzed by the unpaired two-sided Student's t test for simple comparisons or one-way ANOVA with Tukey's post hoc test for multiple groups.





(legend on next page)

Article



activity score (NAS) score and the number of inflammatory foci were significantly increased in IL-18BP KO mice (Figure 3D). In addition, more infiltration of inflammatory monocyte-derived cells (MDCs) and IFN γ -positive CD4 and CD8 T cells was observed in the livers of KO FPC mice (Figures 3E and S3E). Remarkably, collagen deposition and the content of liver hydroxyproline were notably augmented in the livers of IL-18BPdeficient mice (Figures 3F and 3G). Immunostaining of α smooth muscle actin (αSMA) and other collagen staining confirmed significant induction of hepatic fibrosis by loss of IL-18BP (Figure S3F). In addition, mRNA expression levels of Ifng, Tnfa, and chemokine (C-C motif) ligand 2 (ccl2) (inflammation-associated genes) and Col1a1, Col3a1, Acta2, and Timp1 (fibrosisassociated genes) were largely upregulated in the livers of KO FPC mice (Figure 3H). Consistently, IL-18 deficiency increased the number of hepatic inflammatory foci and collagen-positive area in MCD diet model of mice (Figure S3G). Altogether, these results suggest that IL-18BP, a natural antagonist of IL-18, is a crucial gatekeeper for inhibiting the progression of hepatic inflammation and fibrosis in MASH models.

Treatment with APB-R3, a long-acting IL-18BP, ameliorates MASH symptoms with attenuation of hepatic inflammation via IFN γ

To test the therapeutic effect of IL-18BP on MASH development, we developed a long-acting human IL-18BP biologics, APB-R3, recombinantly fused with an anti-Serum Albumin Fragment antigen-binding (Fab)-Associated (SAFA) that could enhance the half-life in rodents and monkeys (Figure 4A). 17 Hepatic outcomes of APB-R3 treatment in mice with FPC diet-induced MASH were assessed with sole or co-administration of anti-steatotic agents (liraglutide; glucagon-like peptide-1 [GLP-1] receptor agonist) because IL-18BP did not alter hepatic steatosis (Figure 3C). Liraglutide is an agonistic peptide analog for GLP-1 receptor (GLP1R) that can decrease liver fat contents by significantly reducing body weight. 18 The ratio of liver/body weight was not markedly reduced by sole treatment with APB-R3, whereas APB-R3 significantly decreased plasma ALT and AST levels (Figures 4B and 4C). APB-R3 did not alter body weights of mice with MASH diet, but liraglutide reduced this parameter (Figures S4A and S4B). Hepatic steatosis was decreased by liraglutide, whereas APB-R3 failed to dramatically reduce lipid accumulation, consistent with results of IL-18BP-deficient livers (Figures 4D and S4C). We further found that plasma free IL-18 levels were elevated in patients with MASH with complications of diabetic mellitus and positive correlations between plasma free IL-18 levels and glucose levels (Figure S4D). However, APB-R3 did not improve parameters of glucose tolerance in mice fed with the FPC diet (Figures S4E and S4F). Interestingly, the impact of APB-R3 was mainly associated with attenuation of liver inflammation such as inflammatory foci and inflammatory MDC infiltration, resulting in prominent attenuation of histological NAS score after co-treatment with APB-R3 and liraglutide (Figures 4E and 4F). Numbers of inflammatory foci were also reduced by APB-R3 in the livers of mice with MCD and CDAA-HFD-induced acute MASH (Figures S5A and S5C). The group with APB-R3 treatment showed slight reductions in hepatic S4G). Cytometric bead array also revealed that pro-inflammatory cytokines such as IL-1α, CCL2, and granulocyte-macrophage colony-stimulating factor (GM-CSF) in systemic plasma were reduced by APB-R3 (Figure 4H).

Next, we investigated the global transcriptomics of vehicle- or APB-R3-treated livers of FPC diet-fed mice. Administration of APB-R3 downregulated mRNA levels of various genes especially those associated with inflammatory responses including type 2 IFN, tumor necrosis factor, and IL-1 regulation (Figures 4I-4K). In particular, downstream genes of IFN signaling were lowered by APB-R3 treatment (Figure 4L). To find whether IFN γ was a major cytokine for APB-R3-mediated suppression of hepatic inflammation, we co-injected IFNy neutralization antibody to completely block IFN_Y actions. Surprisingly, the beneficial effects of anti-IFN γ in attenuating MASH were changed into harmful effects, which enhanced plasma ALT/AST levels and hepatic inflammation when APB-R3 was co-injected (Figures 4M-4O). These results indicate that APB-R3 can inhibit inflammatory progression of MASH by decreasing the production of IFN γ , a downstream cytokine of IL-18.

APB-R3 prevents the progression of hepatic fibrosis via HSC inactivation

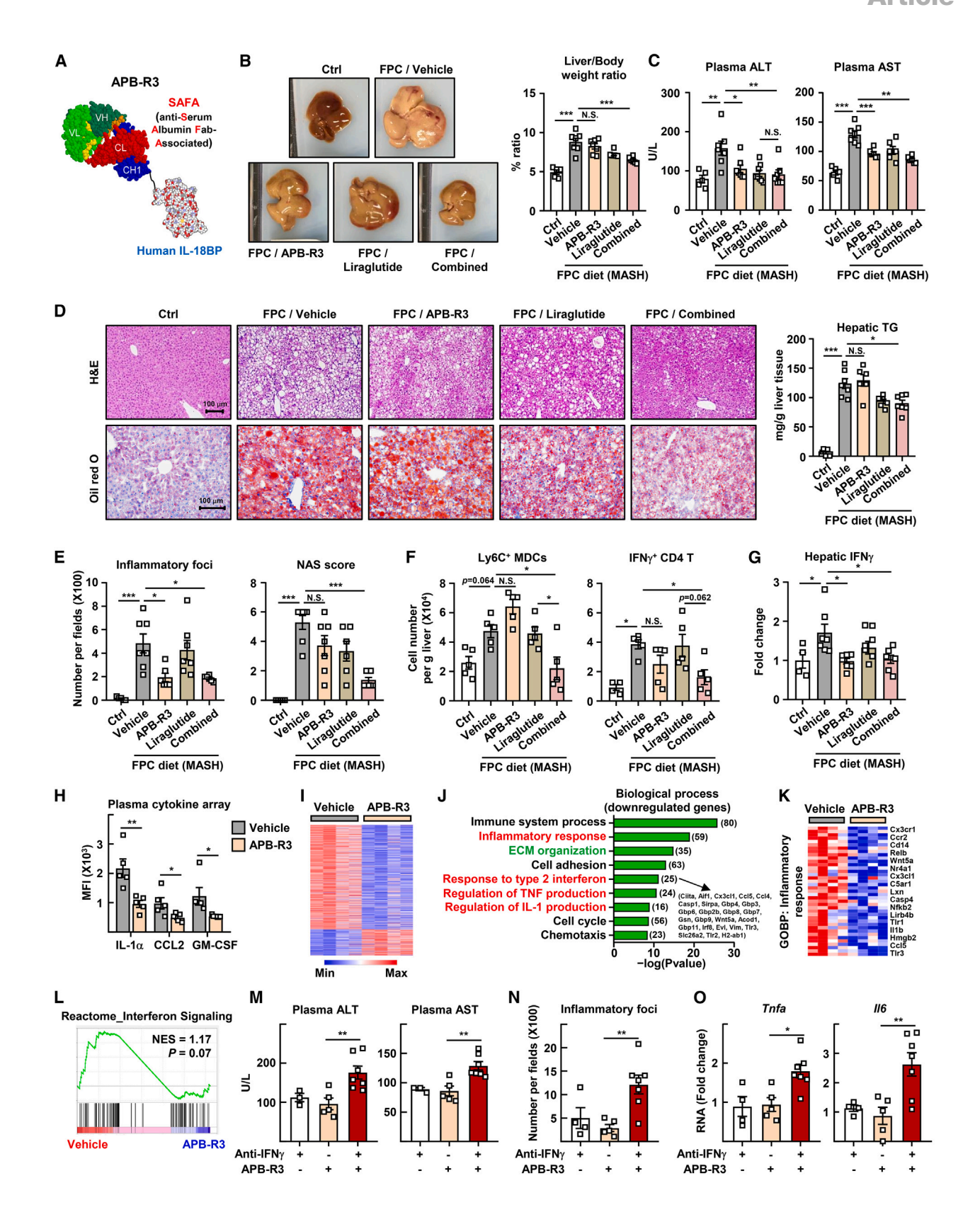
Liver sections from FPC diet-induced MASH mice displayed that APB-R3 treatment strikingly abolished collagen accumulation and sinusoidal fibrosis (Figures 5A and 5B). However, sole treatment with liraglutide failed to eradicate the regions of periportal and pericentral fibrosis (Figures 5A and 5B). Collagen staining using Masson's trichrome confirmed an anti-fibrotic effect of APB-R3 on MASH (Figure 5C). Effects of APB-R3 on hepatic collagen deposition were also observed in MCD and CDAA-HFD diet-fed mice (Figures S5A-S5E). Levels of hepatic hydroxyproline and plasma procollagen type III N-terminal (Pro-C3) as biomarkers of liver fibrosis were also decreased in

Figure 3. Knockout of IL-18BP worsens liver inflammation and fibrosis in MASH models

8-week-old C57BL/6J wild-type (WT) and IL-18BP knockout (KO) mice were fed chow or FPC diet for 15 weeks.

- (A) Representative captured livers (left) and the liver/body weight ratio at the end of experiments (right).
- (B) Measurement of plasma ALT and AST levels.
- (C) H&E and oil red O-stained liver sections (left). Scale bar, 100 μm . Hepatic TG levels were measured (right).
- (D) NAS score and numbers of inflammatory foci of liver histology.
- (E) The numbers of Ly6Chi monocyte-derived cells (MDCs) were analyzed by flow cytometry in the liver.
- (F) Sirius red-stained liver sections (left). Scale bar, 100 μm. Stained positive area was measured by ImageJ (right).
- (G) Measurement of hepatic hydroxyproline.
- (H) Measurement of mRNA levels of pro-inflammatory and fibrosis genes such as Ifng, Tnfa, Cc/2, Col1a1, Col3a1, Acta2, and Timp1 in the liver.
- *p < 0.05, **p < 0.01, and ***p < 0.001. The data represent mean \pm SEM. n = 5–11 per mice group. The data were analyzed by one-way ANOVA with Tukey's post hoc test for multiple groups.





(legend on next page)

Article



APB-R3-treated mice (Figures 5D and 5E). Immunostaining of collagen type 1, aSMA, and desmin revealed that fibrotic activation of HSCs was inhibited by APB-R3 treatment (Figure 5F). APB-R3 also reduced the hepatic expression of αSMA (Figures 5G and S5F). Transcriptomic analysis revealed that APB-R3 broadly downregulated the transcription levels of genes associated with ECM organization and collagen biosynthetic process, indicating that APB-R3 treatment could reduce mRNA levels of hepatic fibrosis genes (Figures 4J, 5H, and 5I). Therefore, APB-R3 combined with anti-steatotic drugs can inhibit the progression of MASH liver with anti-lipid and -fibrosis effects (Figures 4 and 5). We further tested the anti-fibrotic effect of APB-R3 in carbon tetrachloride (CCI₄)-induced hepatic fibrosis model. Administration of APB-R3 remarkably alleviated the formation of bridging fibrosis and collagen deposition (Figures 5J and S5G). αSMA-positive area in the liver was also reduced after APB-R3 administration (Figures 5K and S5G). APB-R3 also reduced diagnostic plasma concentrations of Pro-C3, indicating that neutralization of IL-18 signaling by our engineered long-acting IL-18BP biologics could prevent hepatic fibrogenesis in toxin-induced liver fibrosis models (Figure 5L).

Next, we examined whether blockade of IL-18 by APB-R3 could suppress the progression of MASH using the stelic animal model (STAM) model in which mice displayed hepatic characteristics of steatosis, ballooning, and inflammation until 12 weeks similar to human MASH.¹⁹ Telmisartan was employed as a positive control with a disease comparator in the STAM model to compare with the effectiveness of APB-R3 because telmisartan could improve hepatic steatosis, inflammation, and fibrosis via the modulation of peroxisome proliferator-activated receptors in a mouse model of STAM (Figure S6A).²⁰ APB-R3 did not significantly decrease the mass of liver weight, although plasma ALT and AST activities were similarly reduced by treatment with APB-R3 and telmisartan (Figures S6B and S6C). Unexpectedly, APB-R3 administration improved hepatic steatosis based on histology and reduction in amounts of TGs unlike other MASH diets, indicating that insulin deficiency of the STAM model might have caused distinct lipid alteration after APB-R3 administration (Figures S6D and S6E). Inflammation markers such as numbers of inflammatory foci, plasma cytokines, and inflammatory gene transcriptions were consistently reduced after APB-R3 treatment (Figures S6F–S6H). Fibrotic attenuation by treatment with APB-R3 relative to the vehicle-treated group was observed (Figures S6I–S6K). APB-R3 effectively downregulated the transcriptional levels of fibrotic marker genes in STAM livers (Figure S6L). Pharmacological effects based on the results of dietand STAM-induced MASH models indicate that APB-R3 is an attractive therapeutic drug to effectively ameliorate MASH development.

IL-18 can directly lead to fibrotic activation of primary HSCs when the NLRP3 inflammasome is activated. 5,12 We found that activated HSCs increased IL-18 secretion by activating NLRP3 pathways (Figures 6A-6C). We observed that IL-18 blockade by APB-R3 incubation notably decreased transcriptional levels of fibrotic gene markers and αSMA expression in both primary mouse HSCs and LX-2 human HSC lines (Figures 6D-6F). Next, we analyzed global transcriptome profiles after APB-R3 treatment and confirmed that APB-R3 altered the transcription levels of many genes in primary HSCs (Figure 6G). DAVID Gene Ontology analysis for downregulated genes by APB-R3 revealed associations with acute-phase response, ECM organization, and so on (Figure 6H). Consistently, APB-R3 downregulated the transcription levels of genes associated with ECM organization and collagen formation (Figures 6I and 6J). Interestingly, Kyoto Encyclopedia of Genes and Genomes (KEGG) pathway analysis found that APB-R3 blocked mRNA transcriptions of specific genes related to the cyclic guanosine monophosphate (cGMP)-protein kinase G (PKG) signaling pathway (Figure 6K). Indeed, treatment of cell-permeable cGMP reversed downregulated fibrosis marker genes caused by incubation with APB-R3, indicating that disturbance of the cGMP-PKG pathway was a key mechanism suppressing the fibrotic activation of HSCs upon APB-R3 treatment (Figure 6L).

Treatment of APB-R3 after severely established MASH ameliorates fibrosis features

Finally, we tested whether APB-R3 could block severe properties of MASH after liver fibrosis was already established. Additionally, we compared therapeutic values of APB-R3 with the Food and Drug Administration (FDA)-approved first-in-class MASH drug, thyroid receptor β (THR β) agonist MGL-3196 (resmetirom) (Figure 7A). 21 APB-R3 did not change mice body

Figure 4. Treatment of APB-R3, a long-acting biologics of IL-18BP, ameliorates MASH symptoms by combination therapy with GLP1R agonist

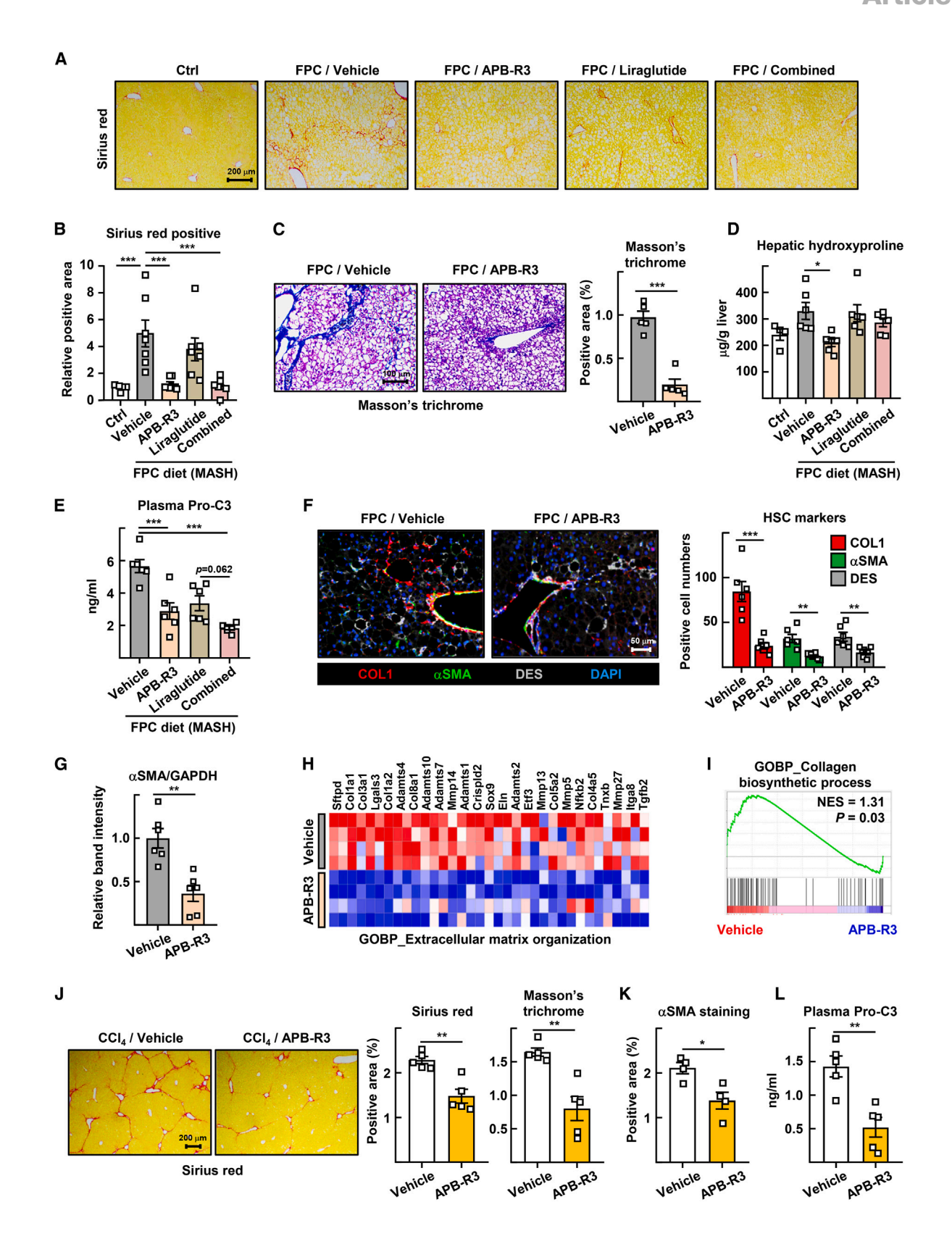
(A–I) C57BL/6J wild-type mice were fed FPC diet for 19 weeks. Drugs were administered from 11 to 19 weeks. 8 mg/kg of APB-R3 (SAFA-hIL-18BP) and/or 100 μ g/kg of GLP1 agonist (Liraglutide) were administered three times a week as indicated. (A) Molecular structure of APB-R3. (B) Representative captured livers (left) and the ratio of liver/body weight (right). (C) Plasma ALT and AST levels were measured at the end of experiments. (D) H&E and oil red O-stained liver sections (left). Scale bar, 100 μ m. The amount of hepatic triglycerides (TGs) was measured (right). (E) The numbers of inflammatory foci and NAS score of liver histology. (F) The numbers of Ly6Chi MDCs and IFN γ -positive CD4 T cells were analyzed by flow cytometry in the liver. (G) ELISA assay was conducted to measure hepatic amounts of IFN γ . (H) Bead cytokine array was conducted for blood plasma. Representative results for IL-1 α , CCL2, and GM-CSF were exhibited. (I) Heatmap analysis of mRNA transcripts of vehicle or APB-R3-treated livers.

- (J) Representative pathways of Gene Ontology enrichment analysis for downregulated genes in APB-R3-treated livers.
- (K) Heatmap analysis of the genes related with inflammatory response in vehicle or APB-R3 administration.
- (L) GSEA analysis for reactome of interferon signaling in vehicle or APB-R3-treated livers.

(M-O) C57BL/6J wild-type mice were fed FPC diet for 19 weeks. Drugs were administered from 11 to 19 weeks. 8 mg/kg of APB-R3 and/or 10 mg/kg of anti-IFN γ were administered three times a week as indicated. (M) Plasma ALT and AST levels were measured at the end of experiments. (N) The numbers of inflammatory foci of liver histology. (O) Measurement of mRNA levels of proinflammatory genes such as *Tnfa* and *ll6* in the livers.

*p < 0.05, **p < 0.01, and ***p < 0.001. The data represent mean \pm SEM. n = 4-8 per mice group. The data were analyzed by one-way ANOVA with Tukey's post hoc test for multiple groups.





(legend on next page)

Article



weight, but MGL-3196 dramatically reduced this parameter (Figure 7B). Also, liver/body weight ratio was not altered by APB-R3, whereas MGL-3196 decreased this ratio, indicating that MGL-3196 improved lipid and ballooning in severe MASH (Figures 7A and 7B). Plasma ALT/AST levels and the number of inflammatory foci were similarly decreased by treatment with APB-R3 and MGL-3196, respectively (Figures 7C and 7D). Surprisingly, APB-R3 could reduce area and amounts of hepatic collagen accumulation than levels of these markers at 19 weeks of MASH (Figures 7E, 7F, and S7A). MGL-3196 showed similar anti-collagen effects, but sinusoidal and periportal fibrosis slightly remained (Figures 7E and S7A). APB-R3 further reduced plasma pro-C3 levels than MGL-3196 (Figure 7G), and expression of αSMA was attenuated by APB-R3 treatment against developed MASH (Figures 7H, S7B, S7C, and S7E). These results suggest that APB-R3 even ameliorates hepatic fibrosis in severely developed MASH similar with the FDA-approved MASH drug, resmetirom.

Finally, after 7 weeks of CCl_4 injection, we started to treat mice with APB-R3 to determine whether APB-R3 could reverse severely progressed liver fibrosis (Figure 7I). Histological analysis revealed that APB-R3 effectively decreased established collagen deposition into properties of early stage of liver fibrosis (Figures 7J, 7K, and S7D). The amount of hepatic collagen was sufficiently reduced by APB-R3 treatment to almost basal levels (Figure 7L). Plasma Pro-C3 levels were also attenuated in this model (Figure 7M). APB-R3 administration after a moderate stage of liver fibrosis significantly decreased hepatic expression of α SMA (Figures 7N and S7C–S7E).

DISCUSSION

In the present study, we found that uncontrolled free-IL-18 in the liver was augmented under the MASH condition to cause severe hepatic inflammation and fibrosis (Figure 1). Although the expression of IL-18BP was also increased, IL-18BP level was not high enough to completely inhibit the activity of IL-18 (Figure 1C). In human plasma, free IL-18 concentrations are higher in patients with MASH than in healthy controls because of slight increases of IL-18BP in patients with MASH, indicating that sufficient elevated amounts of IL-18BP are needed to block MASH development (Figure 1H). Indeed, free IL-18 levels are elevated and correlated with degrees of chronic liver diseases including MASH and fibrosis (Figures 1E and 1I). We newly discovered that hepatocytes were major sources of IL-18BP in the liver via

a regulatory feedback mechanism of IL-18 stimulation for IFN $_{\Upsilon}$ production in CD4 T cells (Figure 2). Interestingly, systemic depletion of IL-18BP resulted in dramatically worsened disease severity of MASH than WT mice, indicating that a feedback mechanism of IL-18BP is an important gatekeeper to inhibit MASH development (Figure 3). Impaired hepatocytes by other stressors including lipotoxicity, oxidative stress, and unfolding protein stress might disturb sufficient production of IL-18BP to completely block IL-18 signaling in MASH. Our results suggest that complete blockade of IL-18 activity by injecting additional exogenous IL-18BP has a great potential to improve IL-18-induced MASH inflammation and fibrosis (Figures 4 and 5).

Previously, some studies have reported that NLRP3 inflammasome activation is responsible for the development of liver inflammation and fibrosis in a MASH mouse model.²² Inflammasome can lead to elevated secretion of inflammatory IL-1ß and IL-18 cytokines, contributing to liver injuries. IL-1β has been proposed as a key player in inflammasome-mediated MASH development. However, many studies have shown unexpected results about the roles of IL-1ß. Treatment with anakinra, an IL-1 receptor antagonist, only reduced hepatic inflammation, whereas it did not alter HSC activation and collagen deposition in the liver. 9 In a mouse model expressing constitutively activated NLRP3 in myeloid cells, IL-1 receptor KO did not prevent the pathogenesis of liver inflammation.²³ In contrast, the roles of IL-18 signaling have been identified and emphasized in liver inflammation and fibrosis. Systemic loss of IL-18 receptor largely diminishes neutrophil accumulation in the liver when NLRP3 is hyperactivated in myeloid cells.²³ IL-18 receptor KO mice also exhibit reduced ALT levels in diet-induced MAFLD models.²⁴ Recently, Knorr et al. have identified the pathogenic roles of IL-18 in liver fibrosis, showing that IL-18 can directly lead to fibrogenic activation of HSCs in hyperactivated NLRP3 mouse models. 12 However, their study used a systemic hyperactivated NLRP3 mouse model, which showed poor growth of mice and did not further investigate the modulation of hepatic inflammation, detailed mechanism, and therapeutic potential in MASH disease. 12 IL-1β and IL-18 cytokines have different downstream signaling pathway in controlling inflammatory response, resulting in a discrepancy in the modulation of fibrosis.²⁵ Here, we found that IL-18 signaling was enhanced in MASH conditions. In this study, we focused on the striking roles of IL-18BP in liver inflammation and fibrosis and determined detailed mechanisms using MASH mouse models with IL-18BP KO mice and an IL-18BP biologics (Figures 3, 4, 5, 6, and 7).

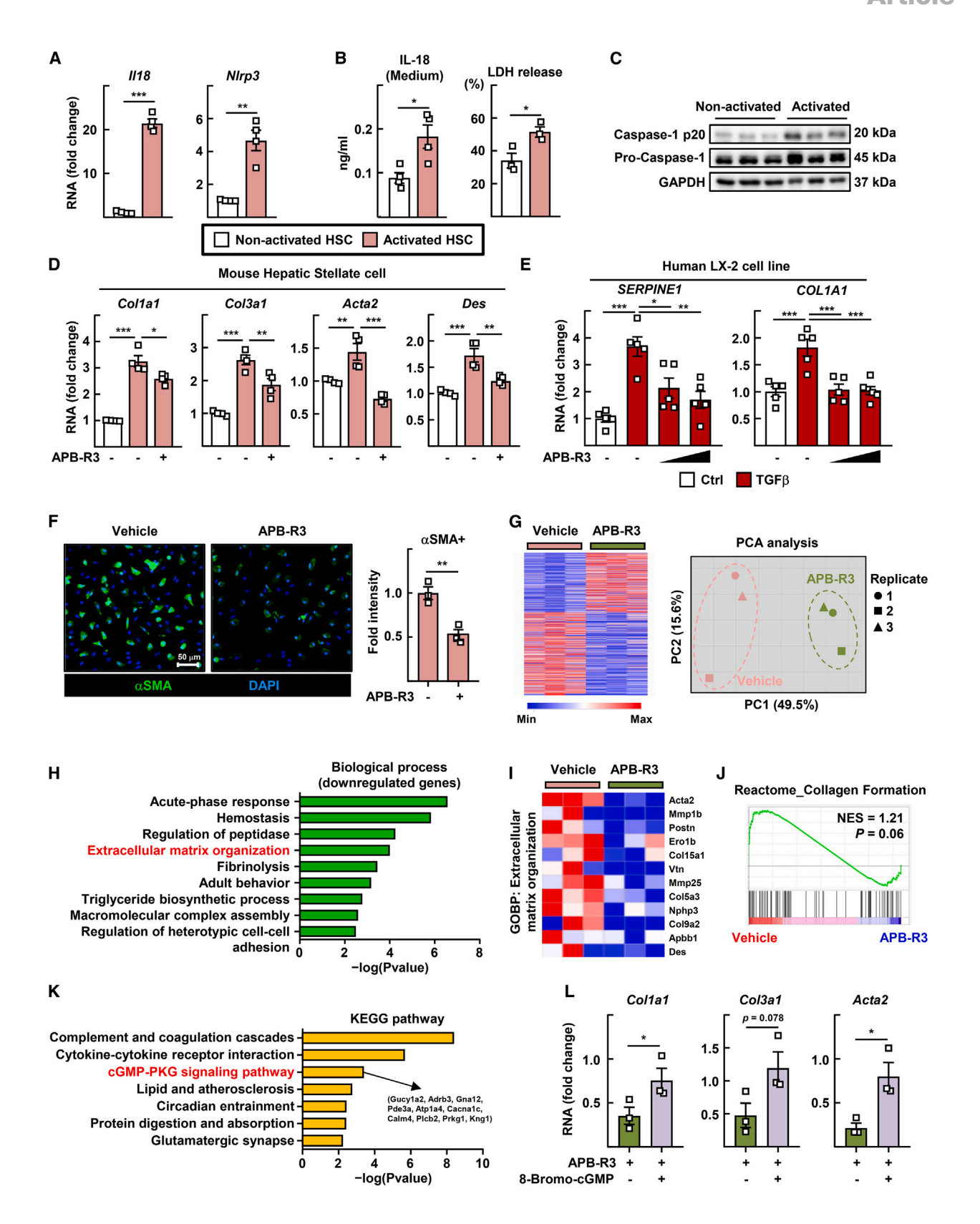
Figure 5. APB-R3 prevents the progression of hepatic fibrosis

(A–I) C57BL/6J wild-type mice were fed FPC diet for 19 weeks. Drugs were administered from 11 to 19 weeks. 8 mg/kg of APB-R3 (SAFA-hIL-18BP) and/or 100 μg/kg of GLP1 agonist (liraglutide) were administered three times a week as indicated. (A) Sirius red-stained liver sections. Scale bar, 200 μm. (B) Relative Sirius red-positive area of liver histology. (C) Masson's trichrome-stained area of liver sections was analyzed. Scale bar, 100 μm. (D) Measurement of hepatic hydroxyproline. (E) ELISA assay was conducted to measure plasma procollagen type III N-terminal (Pro-C3). (F) Immunostaining of liver section for collagen type 1 (COL1), αSMA, and desmin (DES) proteins. Stained cell numbers were counted. Scale bar, 50 μm. (G) Relative band intensity of αSMA protein in the liver was measured. (H) Heatmap analysis of the genes related with extracellular matrix organization in vehicle or APB-R3 administration. (I) GSEA analysis for Gene Ontology of collagen biosynthetic process in vehicle or APB-R3-treated livers.

(J–L) C57BL/6J wild-type mice were administered with carbon tetrachloride (CCl₄) for 5 weeks. 8 mg/kg of APB-R3 or PBS was administered three times a week at 3 to 5 weeks. (J) Sirius red and Masson's trichrome-stained liver sections were presented and positive area was analyzed by ImageJ. Scale bar, 200 μ m. (K) Immunostaining of liver section for α SMA proteins. Stained area was measured. (L) ELISA assay was conducted to measure plasma Pro-C3.

*p < 0.05, **p < 0.01, and ***p < 0.001. The data represent mean \pm SEM. n = 4-8 per mice group. The data were analyzed by the unpaired two-sided Student's t test for simple comparisons or one-way ANOVA with Tukey's post hoc test for multiple groups.





(legend on next page)

Article



We found that the presence of APB-R3 in vitro directly suppressed fibrogenic activation of HSCs (Figure 6). Activation of canonical NLRP3 inflammasome in HSCs can release IL-18 cytokines. The released IL-18 can further increase mRNA levels of profibrotic genes.^{5,12} HSC-specific persistent activation of NLRP3 can alter quiescent status toward activated HSCs, resulting in exacerbated phenotypes of hepatic inflammation and fibrosis.⁵ Therefore, APB-R3 can interrupt the self-boosting IL-18 signaling and effectively inhibit the fibrogenic activation of HSCs in vitro (Figures 6A-6F). Blockade of IL-1β by treatment with anakinra reduced the proliferative function of primary HSCs. However, anakinra unexpectedly worsened hepatic fibrosis in a CCI₄-injected mouse model in vivo. ^{26,27} In contrast, our findings indicated that APB-R3 largely diminished the development of fibrogenesis both in vitro and in vivo. We further explored detailed molecular mechanisms of how IL-18 blockade inhibited the activation of HSCs. Blockade of self-released IL-18 resulted in inhibition of the cGMP-PKG signaling pathway to suppress HSC activation (Figures 6K and 6L). Indeed, the cGMP-PKG pathway can contribute to the modulation of HSC activation.²⁸ Therefore, administration of IL-18BP biologics provides a beneficial therapeutic strategy because APB-R3 can directly suppress hepatic fibrogenesis of HSCs by inhibiting NLRP3mediated IL-18 self-boosting and cGMP signaling pathways.

IL-18 and IL-18BP can be systemically circulated in our body. Several studies have reported physiological roles of IL-18BP in other tissues. IL-18 deficiency can promote insulin resistance and obesity. Transgenic overexpression of IL-18BP can result in a slight induction of insulin tolerance, suggesting harmful functions of IL-18BP.²⁹ However, impaired balance of IL-18 and IL-18BP can lead to uncontrolled inflammatory diseases in other tissues. IL-18BP plays an important role in inducing goblet cell maturation in colitis diseases by blocking IL-18 activity. Thus, recombinant IL-18BP can effectively attenuate intestinal damages in a dextran sulfate sodium-induced colitis model. 30,31 Furthermore, neutralization of IL-18 by exogenous IL-18BP administration can largely decrease the severity of rheumatoid arthritis.³² To apply IL-18BP therapy clinically, we newly engineered a long-acting IL-18BP biologics and recently reported that APB-R3 could efficiently attenuate IL-18-induced macrophage activation syndrome in the spleen and atopic dermatitis of the skin. 17 Indeed, a human-usable anti-IL-18 monoclonal antibody, GSK- 1070806, is under clinical development for Crohn's disease and atopic dermatitis (NCT03681067; NCT06447506). However, effects of therapeutic drugs such as GSK-1070806 and APB-R3 on MASH should be tested in the near future. In the present study, we further proved that APB-R3 was an effective agent that could alleviate liver inflammation and fibrosis in diverse MASH mouse models, suggesting that APB-R3 drug could be an attractive pharmaceutical agent to relieve numerous IL-18-related inflammatory diseases with broad clinical usages (Figures 4, 5, 6, and 7).

Here, we newly developed biologics to block IL-18 signaling through SAFA platform conjugation with IL-18BP (Figure 4A). APB-R3 has several attractive advantages to be used as a MASH therapy clinically. First, analysis of pK parameters identified that the half-life of APB-R3 in monkeys was extended to approximately 7 days because of the SAFA platform, suggesting that injection of APB-R3 at interval of one time a week would be possible in the human as well. 17 Improved stability of biologics can provide better competitiveness in the development of clinically usable drugs. Second, we confirmed that APB-R3 did not have any severe side effects or toxicity. We measured whole body weight changes and found no differences in weight changes of mice with several MASH diets under APB-R3 treatment (Figures S4A and S4B). We also found that APB-R3 did not affect the function of innate immunity (data not shown). In addition, APB-R3 was found to be safe in rat, non-human primate, and human. This indicates that APB-R3 does not have pharmacologically toxic properties (data not shown). Indeed, in a phase 1 clinical study for human (NCT05715736) to check its safety, no adverse effects were confirmed by APB-R3 administration. Third, we are suspecting that SAFA platforms could support a preferential delivery of APB-R3 into the liver because SAFA can easily bind to hepatic albumin, resulting in effective inhibition of local hepatic IL-18 signaling. These drug properties support potential clinical development of APB-R3 for curing MASH.

Recently, numerous pipelines to cure MASH and liver fibrosis have been developed by many pharmaceutical companies. Obeticholic acid, a farnesoid X receptor agonist, was clinically tested in phase 2 and phase 3 trials. It resulted in effective resolution of MASH and fibrosis.³³ However, FDA rejected the approval of obeticholic acid because long-term administration of obeticholic

Figure 6. Blockade of IL-18 ameliorates fibrotic activation of hepatic stellate cells via cGMP signaling pathway

- (A) Measurement of mRNA levels of II18, and NIrp3 in non-activated (day 3) and activated (day 5) primary hepatic stellate cells (HSCs).
- (B) The concentrations of IL-18 in HSCs medium were measured (left). Lactate dehydrogenase (LDH) release assay in cell medium was conducted (right).
- (C) Representative immunoblot analysis in cell medium for caspase-1 p20 and lysates for pro-caspase-1 and housekeeping proteins from HSCs were conducted. (D) Measurement of mRNA levels of fibrosis genes such as *Col1a1*, *Col3a1*, *Acta2*, and *Des* in non-activated (day 3) and activated (day 5) primary HSCs. APB-R3 was treated at day 4 for 18 h
- (E) Measurement of mRNA levels of genes related with LX-2 cell activation such as SERPINE1 and COL1A1 in control and TGF-β-treated human LX-2 cell lines.
- (F) Immunofluorescence images of primary HSCs for αSMA. Scale bar, 50 μm. αSMA-positive area was analyzed.
- (G) Heatmap and principal component analysis (PCA) analysis of mRNA transcripts of vehicle or APB-R3-treated HSCs.
- (H) Representative pathways of Gene Ontology enrichment analysis for downregulated genes in APB-R3-treated HSCs.
- (I) Heatmap analysis of the genes related with extracellular matrix organization in vehicle or APB-R3 incubation.
- (J) GSEA analysis for reactome of collagen formation in vehicle or APB-R3-treated HSCs.
- (K) Representative KEGG pathways for downregulated genes in APB-R3-treated HSCs.
- (L) Measurement of mRNA levels of fibrosis genes such as Col1a1, Col3a1, and Acta2, in vehicle or 8-bromo-cGMP incubation on APB-R3-treated HSCs.
- *p < 0.05, **p < 0.01, and ***p < 0.001. The data represent mean \pm SEM. n = 3–5 per experimental condition. The data were analyzed by the unpaired two-sided Student's t test for simple comparisons or one-way ANOVA with Tukey's post hoc test for multiple groups.



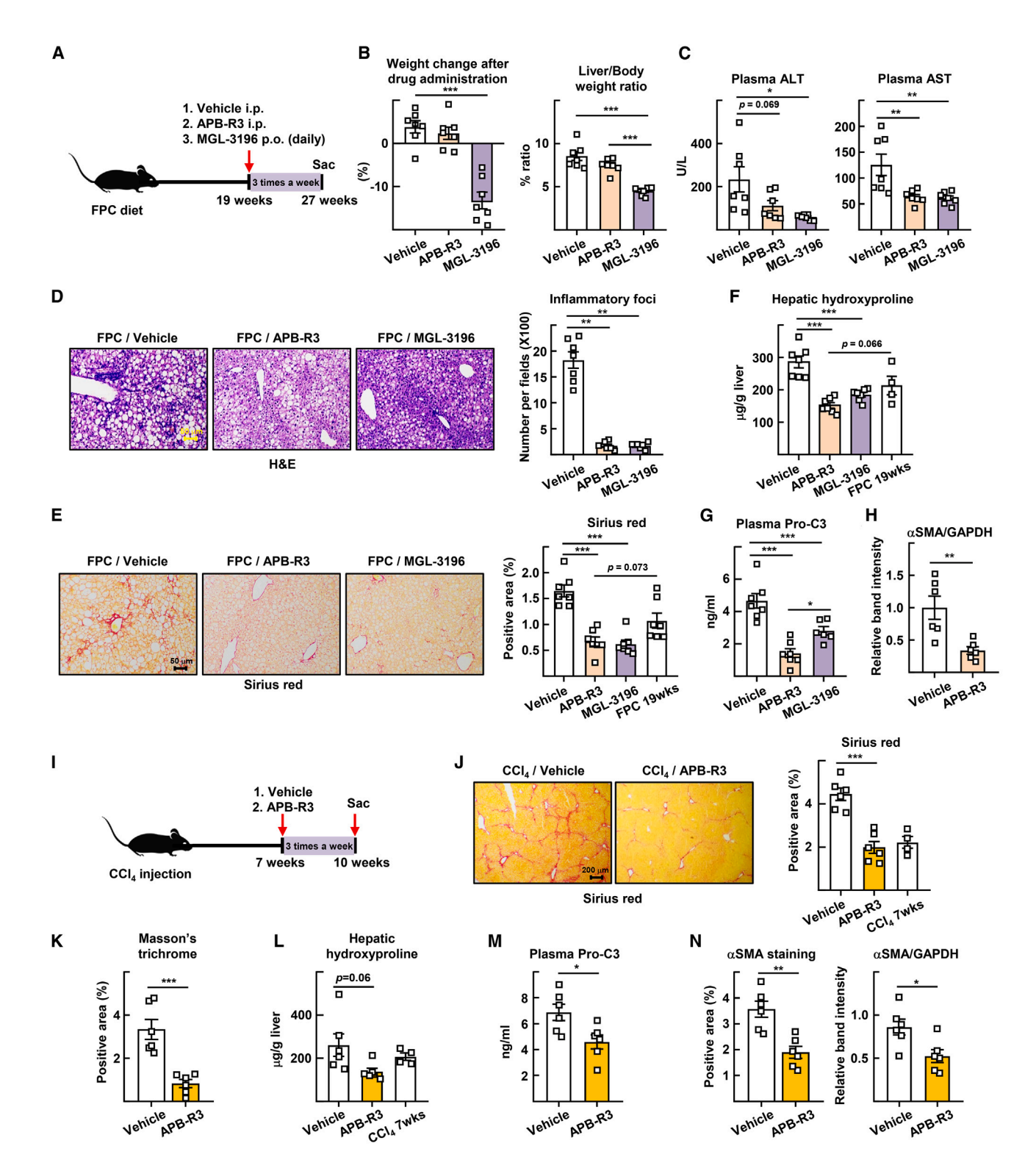


Figure 7. APB-R3 treatment after establishment of liver fibrosis ameliorates disease parameters

(A) C57BL/6J wild-type mice were fed FPC diet for 27 weeks. Drugs were administered from 19 to 27 weeks. 8 mg/kg of APB-R3 (SAFA-hlL-18BP) was intraperitoneally administered three times a week as indicated. 5 mg/kg of THRβ agonist (MGL-3196; resmetirom) was daily orally gavaged as compared group. (B) Body weight change after drug administration was measured at the end of experiments (left). The ratio of liver/body weight was analyzed (right). (C) Plasma ALT and AST levels were measured at the end of experiments.

Article



acid had severe side effects such as pruritus and increased plasma cholesterols (NCT02548351). Madrigal pharmaceuticals have developed resmetirom, a liver-directed selective THRB agonist that targets MASH.34 Resmetirom reduced ALT and AST levels, liver fat contents, and fibrosis in phase 3 trials without any remarkable side effects, finally leading to the approved firstin-class drug targeting MASH (NCT03900429).21 Based on mechanisms of resmetirom by enhancing the breakdown of lipids, hepatic fatty liver was dramatically improved compared to placebo. However, its anti-fibrotic effects were not evident in that only about 10% of resmetirom-treated patients showed fibrosis improvement compared to placebo.²¹ We compared anti-fibrosis effects of resmetirom and APB-R3 and showed an additional reduction in accumulated collagen deposition in the severely developed MASH model (Figures 7E and 7F). MASH is a multifactorial disease involving diverse mechanisms of hepatic steatosis, inflammation, and fibrosis, indicating that combination therapy targeting multiple liver mechanisms is a promising option for MASH. 35,36 In particular, regression of hepatic fibrotic regions is an important issue because catastrophic cirrhosis contributes to MASH-related mortality. Our results suggest that APB-R3 could neutralize IL-18 activity and lead to positive outcomes by strikingly diminishing hepatic fibrosis and inflammation even against developed MASH (Figures 4, 5, 6, and 7). Knorr et al. have reported that treatment with recombinant human IL-18BP (tadekinig alfa) can reduce collagen deposition in overactivated NLRP3-mediated injured liver. 12 APB-R3 is an improved biologics of human IL-18BP, which shows prolonged stability and comparable bioactivity in blocking IL-18 signaling compared with tadekinig alfa via fusion with anti-albumin Fab. 17 Our results demonstrate that sole treatment with APB-R3 has therapeutic potential to ameliorate liver inflammation and fibrosis under a MASH condition. Therefore, synergistic combination therapy with GLP1R agonist and APB-R3 prominently reversed MASH-injured livers almost toward a normal histologic status (Figure 4). In summary, combining anti-steatotic agents and anti-fibrotic APB-R3 could be an attractive therapeutic option against MASH. This study provides new insight into clinical approaches of inflammasome regulator and IL-18BP biologics for treating MASH.

Limitations of the study

This study concluded that CD4 $^+$ T cells uniquely contribute to increased IFN $_{\Upsilon}$ production in response to IL-18 within the IL-18/CD4 T/IL-18BP regulatory axis in the MASH model. However,

the specific mechanisms and factors that make CD4 T cells the exclusive responders secreting IFN γ upon IL-18 stimulation remain unclear and are required to further investigation to elucidate the selective response of these cells in the context of MASH progression. While our findings demonstrate that APB-R3 reduces HSC activation through downregulation of genes associated with the cGMP-PKG signaling pathway, the potential involvement of additional pathways in HSC activation remains unexplored. Further studies are needed to investigate whether other signaling pathways also contribute to the modulation of HSC activation by IL-18 blockade.

RESOURCE AVAILABILITY

Lead contact

Further information and requests for resources and reagents should be directed to and will be fulfilled by the lead contact, Yong-Hyun Han (yhhan1015@kangwon.ac.kr).

Materials availability

Other materials in this study are available from the lead contact without restriction. C57BL/6 IL-18BP KO mice in this study are available from the lead contact with a completed Materials Transfer Agreement. There are restrictions to the availability of APB-R3 due to the lack of an external centralized repository for its distribution and our upcoming conflict issue in clinical development. We are glad to share APB-R3 with reasonable compensation by requestor for its processing and shipping.

Data and code availability

- The novel RNA-seq raw data described in this publication have been deposited in NCBI's Gene Expression Omnibus (GEO) and are publicly accessible through GEOSeries accession number: GSE279496 (https:// www.ncbi.nlm.nih.gov/geo/query/acc.cgi?acc=GSE279496) and GSE 279499 (https://www.ncbi.nlm.nih.gov/geo/query/acc.cgi?acc=GSE 279499).
- This paper analyzes existing, publicly available data sourced from GEO: GSE61260. These accession numbers for the datasets are listed in the key resources table. All data reported in this paper will be shared by the lead contact upon reasonable request.
- No custom code is reported here.
- Any additional information required to reanalyze the data reported in this
 paper is available from the lead contact upon request.

ACKNOWLEDGMENTS

This work was supported by a National Research Foundation of Korea (NRF) grant funded by the Korean government (RS-2024-00338402, RS-2024-00439637, and 2022R1A6C101A739 to Y.-H.H., RS-2024-00413453 to D.-H.K., and 2021R1A2C1012421 to S.G.K.), the Global-Learning & Academic research institution for Master's PhD students and Postdocs (LAMP) Program

- (D) Representative images of H&E liver sections (left). Scale bar, 50 µm. The numbers of inflammatory foci of liver histology (right).
- (E) Representative images of Sirius red-stained liver sections. Scale bar, 50 µm. Sirius red-positive area of liver histology was measured.
- (F) Measurement of hepatic hydroxyproline.
- (G) ELISA assay was conducted to measure plasma Pro-C3.
- (H) Relative band intensity of αSMA protein in the liver was measured.
- (I) C57BL/6J wild-type mice were administered with carbon tetrachloride (CCl₄) for 10 weeks. 8 mg/kg of APB-R3 or PBS was administered three times a week at 7 to 10 weeks
- (J and K) Sirius red and Masson's trichrome-stained liver sections were presented and positive area was analyzed by ImageJ. Scale bar, 200 µm.
- (L) Measurement of hepatic hydroxyproline.
- (M) ELISA assay was conducted to measure plasma Pro-C3.
- (N) Immunostaining of liver section for α SMA proteins. Stained area was measured (left). Relative band intensity of α SMA protein in the liver was measured (right). *p < 0.05, **p < 0.01, and ***p < 0.001. The data represent mean \pm SEM. n = 4-7 per mice group. The data were analyzed by the unpaired two-sided Student's t test for simple comparisons or one-way ANOVA with Tukey's post hoc test for multiple groups.



of the National Research Foundation of Korea (NRF) grant funded by the Ministry of Education (RS-2023-00301850), and the internal research fund from AprilBio Co., Ltd. The graphical abstract was created with BioRender.com.

AUTHOR CONTRIBUTIONS

D.-H.K., G.C., E.-B.S., H.L., J.K., and Y.-S.J. performed the experiments, analyzed the results, and prepared figures. J.P., S.C., J.H., and S.-M.K. conducted the experiments producing APB-R3 biologics. D.K. discussed biologics and revised the manuscripts. S.H.B. reviewed the draft and discussed the data. H.W.L. and J.Y.P. provided human samples. D.-H.K., G.C., E.-B.S., H.L., J.K., S.G.K., and Y.-H.H. wrote and revised the manuscript. Y.-H.H., S.-H.C., and S.G.K. conceived, designed, and supervised the research.

DECLARATION OF INTERESTS

At the time of submission, J.P., S.C., J.H., S.-M.K., and S.-H.C. were employees of AprilBio Co., Ltd (Chuncheon, South Korea).

STAR*METHODS

Detailed methods are provided in the online version of this paper and include the following:

- KEY RESOURCES TABLE
- EXPERIMENTAL MODEL AND STUDY PARTICIPANT DETAILS
 - Study approval
 - o Human samples and group information
 - Animal experiments
 - $_{\odot}\,$ Isolation and culture of hepatic stellate cells
- METHOD DETAILS
 - Glucose tolerance test
 - $\,\circ\,$ Staining of stellate cells and sectioned liver tissues
 - o Quantitative real-time PCR (qRT-PCR)
 - Immunoblot
 - o Enzyme-linked immunosorbent assay (ELISA)
 - Flow cytometry
 - Plasma cytokine assay
 - Measurement of hepatic triglycerides (TGs) and plasma biochemistry
 - $\,\circ\,$ Measurement of hepatic hydroxyproline
 - \circ RNA isolation for sequencing
 - Library preparation and sequencing (mRNA-seq)
 - Library preparation and sequencing (QuantSeq)
 - O Data analysis for RNA-seq
- QUANTIFICATION AND STATISTICAL ANALYSIS

SUPPLEMENTAL INFORMATION

Supplemental information can be found online at https://doi.org/10.1016/j.xcrm.2025.102047.

Received: October 7, 2023 Revised: October 18, 2024 Accepted: March 7, 2025 Published: April 15, 2025

REFERENCES

 Singh, S., Allen, A.M., Wang, Z., Prokop, L.J., Murad, M.H., and Loomba, R. (2015). Fibrosis progression in nonalcoholic fatty liver vs nonalcoholic steatohepatitis: a systematic review and meta-analysis of paired-biopsy studies. Clin. Gastroenterol. Hepatol. 13, 643-e40. https://doi.org/10. 1016/j.cgh.2014.04.014.

- Estes, C., Razavi, H., Loomba, R., Younossi, Z., and Sanyal, A.J. (2018). Modeling the epidemic of nonalcoholic fatty liver disease demonstrates an exponential increase in burden of disease. Hepatology 67, 123–133. https://doi.org/10.1002/hep.29466.
- Anstee, Q.M., Targher, G., and Day, C.P. (2013). Progression of NAFLD to diabetes mellitus, cardiovascular disease or cirrhosis. Nat. Rev. Gastroenterol. Hepatol. 10, 330–344. https://doi.org/10.1038/nrgastro.2013.41.
- Tsuchida, T., and Friedman, S.L. (2017). Mechanisms of hepatic stellate cell activation. Nat. Rev. Gastroenterol. Hepatol. 14, 397–411. https://doi.org/10.1038/nrgastro.2017.38.
- Inzaugarat, M.E., Johnson, C.D., Holtmann, T.M., McGeough, M.D., Trautwein, C., Papouchado, B.G., Schwabe, R., Hoffman, H.M., Wree, A., and Feldstein, A.E. (2019). NLR Family Pyrin Domain-Containing 3 Inflammasome Activation in Hepatic Stellate Cells Induces Liver Fibrosis in Mice. Hepatology 69, 845–859. https://doi.org/10.1002/hep.30252.
- Zisser, A., Ipsen, D.H., and Tveden-Nyborg, P. (2021). Hepatic Stellate Cell Activation and Inactivation in NASH-Fibrosis-Roles as Putative Treatment Targets? Biomedicines 9, 365. https://doi.org/10.3390/biomedicines 9040365.
- Harel, M., Fauteux-Daniel, S., Girard-Guyonvarc'h, C., and Gabay, C. (2022). Balance between Interleukin-18 and Interleukin-18 binding protein in auto-inflammatory diseases. Cytokine 150, 155781. https://doi.org/10. 1016/j.cyto.2021.155781.
- Park, S.Y., Hisham, Y., Shin, H.M., Yeom, S.C., and Kim, S. (2022). Inter-leukin-18 Binding Protein in Immune Regulation and Autoimmune Diseases. Biomedicines 10, 1750. https://doi.org/10.3390/biomedicines10071750
- Wree, A., Eguchi, A., McGeough, M.D., Pena, C.A., Johnson, C.D., Canbay, A., Hoffman, H.M., and Feldstein, A.E. (2014). NLRP3 inflammasome activation results in hepatocyte pyroptosis, liver inflammation, and fibrosis in mice. Hepatology 59, 898–910. https://doi.org/10.1002/hep.26592.
- Gaul, S., Leszczynska, A., Alegre, F., Kaufmann, B., Johnson, C.D., Adams, L.A., Wree, A., Damm, G., Seehofer, D., Calvente, C.J., et al. (2021). Hepatocyte pyroptosis and release of inflammasome particles induce stellate cell activation and liver fibrosis. J. Hepatol. 74, 156–167. https://doi.org/10.1016/j.jhep.2020.07.041.
- Mridha, A.R., Wree, A., Robertson, A.A.B., Yeh, M.M., Johnson, C.D., Van Rooyen, D.M., Haczeyni, F., Teoh, N.C.H., Savard, C., Ioannou, G.N., et al. (2017). NLRP3 inflammasome blockade reduces liver inflammation and fibrosis in experimental NASH in mice. J. Hepatol. 66, 1037–1046. https://doi.org/10.1016/j.jhep.2017.01.022.
- Knorr, J., Kaufmann, B., Inzaugarat, M.E., Holtmann, T.M., Geisler, L., Hundertmark, J., Kohlhepp, M.S., Boosheri, L.M., Chilin-Fuentes, D.R., Birmingham, A., et al. (2023). Interleukin-18 signaling promotes activation of hepatic stellate cells in mouse liver fibrosis. Hepatology 77, 1968–1982. https://doi.org/10.1002/hep.32776.
- Castillo-Dela Cruz, P., Wanek, A.G., Kumar, P., An, X., Elsegeiny, W., Horne, W., Fitch, A., Burr, A.H.P., Gopalakrishna, K.P., Chen, K., et al. (2019). Intestinal IL-17R Signaling Constrains IL-18-Driven Liver Inflammation by the Regulation of Microbiome-Derived Products. Cell Rep. 29, 2270–2283.e7. https://doi.org/10.1016/j.celrep.2019.10.042.
- Ludwiczek, O., Kaser, A., Novick, D., Dinarello, C.A., Rubinstein, M., Vogel, W., and Tilg, H. (2002). Plasma levels of interleukin-18 and interleukin-18 binding protein are elevated in patients with chronic liver disease. J. Clin. Immunol. 22, 331–337. https://doi.org/10.1023/a:1020600230977.
- Faggioni, R., Cattley, R.C., Guo, J., Flores, S., Brown, H., Qi, M., Yin, S., Hill, D., Scully, S., Chen, C., et al. (2001). IL-18-binding protein protects against lipopolysaccharide- induced lethality and prevents the development of Fas/Fas ligand-mediated models of liver disease in mice. J. Immunol. 167, 5913–5920. https://doi.org/10.4049/jimmunol.167. 10.5913.
- Im, Y.R., Hunter, H., de Gracia Hahn, D., Duret, A., Cheah, Q., Dong, J., Fairey, M., Hjalmarsson, C., Li, A., Lim, H.K., et al. (2021). A Systematic

Article



- Review of Animal Models of NAFLD Finds High-Fat, High-Fructose Diets Most Closely Resemble Human NAFLD. Hepatology 74, 1884–1901. https://doi.org/10.1002/hep.31897.
- Jang, Y.S., Lee, K., Park, M., Joo Park, J., Choi, G.M., Kim, C., Dehkohneh, S.B., Chi, S., Han, J., Song, M.Y., et al. (2023). Albumin-binding recombinant human IL-18BP ameliorates macrophage activation syndrome and atopic dermatitis via direct IL-18 inactivation. Cytokine 172, 156413. https://doi.org/10.1016/j.cyto.2023.156413.
- Petit, J.M., Cercueil, J.P., Loffroy, R., Denimal, D., Bouillet, B., Fourmont, C., Chevallier, O., Duvillard, L., and Vergès, B. (2017). Effect of Liraglutide Therapy on Liver Fat Content in Patients With Inadequately Controlled Type 2 Diabetes: The Lira-NAFLD Study. J. Clin. Endocrinol. Metab. 102, 407–415. https://doi.org/10.1210/jc.2016-2775.
- Saito, K., Uebanso, T., Maekawa, K., Ishikawa, M., Taguchi, R., Nammo, T., Nishimaki-Mogami, T., Udagawa, H., Fujii, M., Shibazaki, Y., et al. (2015). Characterization of hepatic lipid profiles in a mouse model with nonalcoholic steatohepatitis and subsequent fibrosis. Sci. Rep. 5, 12466. https://doi.org/10.1038/srep12466.
- Park, J.G., Mok, J.S., Han, Y.I., Park, T.S., Kang, K.W., Choi, C.S., Park, H.D., and Park, J. (2019). Connectivity mapping of angiotensin-PPAR interactions involved in the amelioration of non-alcoholic steatohepatitis by Telmisartan. Sci. Rep. 9, 4003. https://doi.org/10.1038/s41598-019-40322-1.
- Harrison, S.A., Bedossa, P., Guy, C.D., Schattenberg, J.M., Loomba, R., Taub, R., Labriola, D., Moussa, S.E., Neff, G.W., Rinella, M.E., et al. (2024). A Phase 3, Randomized, Controlled Trial of Resmetirom in NASH with Liver Fibrosis. N. Engl. J. Med. 390, 497–509. https://doi.org/10. 1056/NEJMoa2309000.
- de Carvalho Ribeiro, M., and Szabo, G. (2022). Role of the Inflammasome in Liver Disease. Annu. Rev. Pathol. 17, 345–365. https://doi.org/10.1146/ annurev-pathmechdis-032521-102529.
- Brydges, S.D., Broderick, L., McGeough, M.D., Pena, C.A., Mueller, J.L., and Hoffman, H.M. (2013). Divergence of IL-1, IL-18, and cell death in NLRP3 inflammasomopathies. J. Clin. Investig. 123, 4695–4705. https:// doi.org/10.1172/jci71543.
- Hohenester, S., Kanitz, V., Schiergens, T., Einer, C., Nagel, J., Wimmer, R., Reiter, F.P., Gerbes, A.L., De Toni, E.N., Bauer, C., et al. (2020). IL-18 but Not IL-1 Signaling Is Pivotal for the Initiation of Liver Injury in Murine Non-Alcoholic Fatty Liver Disease. Int. J. Mol. Sci. 21, 8602. https://doi.org/10. 3390/ijms21228602.
- Lee, J.K., Kim, S.H., Lewis, E.C., Azam, T., Reznikov, L.L., and Dinarello, C.A. (2004). Differences in signaling pathways by IL-1beta and IL-18. Proc. Natl. Acad. Sci. USA 101, 8815–8820. https://doi.org/10.1073/pnas.0402800101.
- Meier, R.P.H., Meyer, J., Montanari, E., Lacotte, S., Balaphas, A., Muller, Y.D., Clément, S., Negro, F., Toso, C., Morel, P., and Buhler, L.H. (2019). Interleukin-1 Receptor Antagonist Modulates Liver Inflammation and Fibrosis in Mice in a Model-Dependent Manner. Int. J. Mol. Sci. 20, 1295. https://doi.org/10.3390/ijms20061295.
- Reiter, F.P., Wimmer, R., Wottke, L., Artmann, R., Nagel, J.M., Carranza, M.O., Mayr, D., Rust, C., Fickert, P., Trauner, M., et al. (2016). Role of interleukin-1 and its antagonism of hepatic stellate cell proliferation and liver fibrosis in the Abcb4(-/-) mouse model. World J. Hepatol. 8, 401–410. https://doi.org/10.4254/wjh.v8.i8.401.
- 28. Perri, R.E., Langer, D.A., Chatterjee, S., Gibbons, S.J., Gadgil, J., Cao, S., Farrugia, G., and Shah, V.H. (2006). Defects in cGMP-PKG pathway

- contribute to impaired NO-dependent responses in hepatic stellate cells upon activation. Am. J. Physiol. Gastrointest. Liver Physiol. 290, 535–542. https://doi.org/10.1152/ajpgi.00297.2005.
- Netea, M.G., Joosten, L.A.B., Lewis, E., Jensen, D.R., Voshol, P.J., Kullberg, B.J., Tack, C.J., van Krieken, H., Kim, S.H., Stalenhoef, A.F., et al. (2006). Deficiency of interleukin-18 in mice leads to hyperphagia, obesity and insulin resistance. Nat. Med. 12, 650–656. https://doi.org/10.1038/nm1415.
- Nowarski, R., Jackson, R., Gagliani, N., de Zoete, M.R., Palm, N.W., Bailis, W., Low, J.S., Harman, C.C.D., Graham, M., Elinav, E., and Flavell, R.A. (2015). Epithelial IL-18 Equilibrium Controls Barrier Function in Colitis. Cell 163, 1444–1456. https://doi.org/10.1016/j.cell.2015.10.072.
- Sivakumar, P.V., Westrich, G.M., Kanaly, S., Garka, K., Born, T.L., Derry, J.M.J., and Viney, J.L. (2002). Interleukin 18 is a primary mediator of the inflammation associated with dextran sulphate sodium induced colitis: blocking interleukin 18 attenuates intestinal damage. Gut 50, 812–820. https://doi.org/10.1136/gut.50.6.812.
- Plater-Zyberk, C., Joosten, L.A., Helsen, M.M., Sattonnet-Roche, P., Siegfried, C., Alouani, S., van De Loo, F.A., Graber, P., Aloni, S., Cirillo, R., et al. (2001). Therapeutic effect of neutralizing endogenous IL-18 activity in the collagen-induced model of arthritis. J. Clin. Investig. 108, 1825–1832. https://doi.org/10.1172/jci12097.
- 33. Younossi, Z.M., Ratziu, V., Loomba, R., Rinella, M., Anstee, Q.M., Goodman, Z., Bedossa, P., Geier, A., Beckebaum, S., Newsome, P.N., et al. (2019). Obeticholic acid for the treatment of non-alcoholic steatohe-patitis: interim analysis from a multicentre, randomised, placebo-controlled phase 3 trial. Lancet 394, 2184–2196. https://doi.org/10.1016/s0140-6736(19)33041-7.
- 34. Kelly, M.J., Pietranico-Cole, S., Larigan, J.D., Haynes, N.E., Reynolds, C.H., Scott, N., Vermeulen, J., Dvorozniak, M., Conde-Knape, K., Huang, K.S., et al. (2014). Discovery of 2-[3,5-dichloro-4-(5-isopropyl-6-oxo-1,6-dihydropyridazin-3-yloxy)phenyl]-3,5-dioxo-2,3,4,5-tetrahydro[1,2,4] triazine-6-carbonitrile (MGL-3196), a Highly Selective Thyroid Hormone Receptor β agonist in clinical trials for the treatment of dyslipidemia. J. Med. Chem. 57, 3912–3923. https://doi.org/10.1021/jm4019299.
- Jeong, S.W. (2020). Nonalcoholic Fatty Liver Disease: A Drug Revolution Is Coming. Diabetes Metab. J. 44, 640–657. https://doi.org/10.4093/dmj. 2020.0115.
- Tincopa, M.A., Anstee, Q.M., and Loomba, R. (2024). New and emerging treatments for metabolic dysfunction-associated steatohepatitis. Cell Metab. 36, 912–926. https://doi.org/10.1016/j.cmet.2024.03.011.
- Han, Y.H., Kim, H.J., Na, H., Nam, M.W., Kim, J.Y., Kim, J.S., Koo, S.H., and Lee, M.O. (2017). RORα Induces KLF4-Mediated M2 Polarization in the Liver Macrophages that Protect against Nonalcoholic Steatohepatitis. Cell Rep. 20, 124–135. https://doi.org/10.1016/j.celrep.2017.06.017.
- Kleiner, D.E., Brunt, E.M., Van Natta, M., Behling, C., Contos, M.J., Cummings, O.W., Ferrell, L.D., Liu, Y.C., Torbenson, M.S., Unalp-Arida, A., et al. (2005). Design and validation of a histological scoring system for nonalcoholic fatty liver disease. Hepatology 41, 1313–1321. https://doi.org/10.1002/hep.20701.
- Younossi, Z.M., Loomba, R., Anstee, Q.M., Rinella, M.E., Bugianesi, E., Marchesini, G., Neuschwander-Tetri, B.A., Serfaty, L., Negro, F., Caldwell, S.H., et al. (2018). Diagnostic modalities for nonalcoholic fatty liver disease, nonalcoholic steatohepatitis, and associated fibrosis. Hepatology 68, 349–360. https://doi.org/10.1002/hep.29721.



STAR***METHODS**

KEY RESOURCES TABLE

REAGENT or RESOURCE	SOURCE	IDENTIFIER
Antibodies		
nVivoMAb rat monoclonal anti-trinitrophenol	BioXcell	Cat# BE0089; RRID: AB_1107769
InVivoMAb Hamster polyclonal anti-IFN γ	Bioxcell	Cat# BE0312; RRID: AB_2736992
nVivoMAb Rat monoclonal anti-CD4	Bioxcell	Cat# BE0003-1; RRID: AB_1107636
nVivoMAb Rat monoclonal anti-CD8	Bioxcell	Cat# BE0061; RRID: AB_1125541
Mouse monoclonal anti-αSMA	Agilent DAKO	Cat# M085129-2; RRID: AB_2811108
Alexa Fluor 488 donkey anti-Mouse	Thermo Fisher	Cat# A-21202; RRID: AB_141607
Goat polyclonal anti-Type I Collagen	Southern Biotech	Cat# 1310-01; RRID: AB_2753206
Rabbit monoclonal anti-Desmin	Abcam	Cat# ab15200; RRID: AB_301744
Alexa Fluor 594 donkey polyclonal anti-goat HRP	Thermo Fisher	Cat# A-11058; RRID: AB_142540
Alexa Fluor 647 donkey anti-Rabbit	Thermo Fisher	Cat# A-31573; RRID: AB_2536183
Rabbit polyclonal anti-GAPDH	Bioss	Cat# bs-2188R; RRID: AB_10856675
Goat anti-mouse HRP	Bio-rad	Cat# 1706516; RRID: AB_2921252
Goat anti-rabbit HRP	Bio-rad	Cat# BR1706515
Rat monoclonal anti-CD16/CD32	BD biosciences	Cat# 553142; RRID: AB_394657
Brilliant Violet786 Rat anti-CD8α	BD Biosciences	Cat# 569395
FITC Rat monoclonal anti-Ly6C	BD Biosciences	Cat# 553104; RRID: AB_394628
PerCP/Cyanine5.5 Rat monoclonal anti-Ly6C	BioLegend	Cat# 128012; RRID: AB_1659241
Brilliant Violet510 Rat monoclonal anti-CD45	BioLegend	Cat# 563891; RRID: AB_2734134
FITC Rat monoclonal anti-CD45	BioLegend	Cat# 103108; RRID: AB_312973
APC-Cy7 Rat monoclonal anti-Ly6G	BioLegend	Cat# 127624; RRID: AB_10640819
APC Rat monoclonal anti-F4/80	BioLegend	Cat# 123116; RRID: AB_893481
PE-Cy7 Rat monoclonal anti-CD11b	BioLegend	Cat# 101215; RRID: AB_312798
Alexa Fluor 488 Rat monoclonal anti-CD44	BioLegend	Cat# 103016; RRID: AB_493679
Alexa Fluor 488 Mouse monoclonal anti-NK1.1	BioLegend	Cat# 108718; RRID: AB_493183
Alexa Fluor 647 Rat monoclonal anti-CD218a (IL-18Rα)	BioLegend	Cat# 157908; RRID: AB_2876539
PerCP/Cyanine5.5 Rat monoclonal anti-CD4	BioLegend	Cat# 100434; RRID: AB_893324
PE Rat monoclonal anti-CD49b	BD Biosciences	Cat# 553858
PerCP/Cyanine5.5 Rat monoclonal anti-CD45R/B220	BioLegend	Cat# 103236; RRID: AB_893354
APC/Fire [™] 750 Hamster monoclonal anti-CD49a	BioLegend	Cat# 142609; RRID: AB_2734203
PE/Cyanine7 Rat monoclonal anti-CD3	BioLegend	Cat# 100220; RRID: AB_1732057
PE Rat monoclonal anti-TIM4	BioLegend	Cat# 130006; RRID: AB_2201843
Jltra-LEAF [™] Purified Hamster nonoclonal anti-CD28	BioLegend	Cat# 102116; RRID: AB_11147170
eFluor [™] 450 Rat monoclonal anti-FOXP	Thermo Fisher	Cat# 48-5773-82; RRID: AB_1518812
Brilliant Violet421 Rat monoclonal anti-IFN γ	BioLegend	Cat# 505830; RRID: AB_2563105
PE Rat monoclonal anti-IFNγ	BioLegend	Cat# 505808; RRID: AB_315402
Biological samples		
Mouse liver paraffin blocks	This paper	N/A
Mouse liver frozen blocks	This paper	N/A
Human blood samples	This paper	IRB No. 4-2015-0184; 4-2020-0504

(Continued on next page)





Continued		
REAGENT or RESOURCE	SOURCE	IDENTIFIER
Chemicals, peptides, and recombinant proteins		
APB-R3	AprilBio Co., Ltd	N/A
Liraglutide	Novo Nordisk	N/A
Carbon tetrachloride	Sigma-Aldrich	Cat# 56-23-5
MGL-3196 (Resmetirom)	MedChemExpress	Cat# HY-12216
D-(+)-Glucose monohydrate	Sigma-Aldrich	Cat# 49159
bovine serum albumin	Sigma-Aldrich	Cat# A8806
Fluoro-Gel II with DAPI	Electron microscopy sciences	Cat# 17985-50
Xylene	Duksan,	Cat# 25165-0480
Eosin Stain Solution, 5% Aqueous	Sigma-Aldrich	Cat# R03040
Picro-Sirius Red solution	Abcam	Cat# ab246832
Heated Oil Red solution	Sigma-Aldrich	Cat# 00625
Easy-BLUE TM	iNtRON	Cat# 17061L
SYBR® Green PCR master mix	Applied Biosystems	Cat# 4367659
RIPA buffer	ELPIS	Cat# EBA-1149
Sodium dodecyl sulfate-polyacrylamide	Bio-rad	Cat# 1610416
gel electrophoresis		
Miracle-Star TM Western Blot Detection System	iNtRON	Cat# 16028
Collagenase D	Sigma-Aldrich	Cat# 11088866001
Percoll	GE Healthcare	Cat# 17-0891-02
Collagenase type IV	Sigma-Aldrich	Cat# C4-BIOC
OptiPrep	Sigma-Aldrich	Cat# D1556
HyClone Dulbecco's Modified Eagle Medium (DMEM) with high glucose: Liquid	Hyclone	Cat# SH30243.01
Trizol reagent	Invitrogen	Cat# 15596026
Murine IL-18	Gibco	Cat# PMC0184
Critical commercial assays		
Human Total IL-18 DuoSet ELISA Kit	R&D systems	Cat# DY318-05
RNeasy mini kit	Qiagen	Cat# 47106
RNeasy Micro kit	Qiagen	Cat# 74004
High-capacity cDNA reverse transcription kit	Thermo Fisher	Cat# 4368814
Mouse IL-18BP ELISA Kit	Abcam	Cat# ab254509
Human IL-18 BPa Quantikine ELISA Kit	R&D systems	Cat# DBP180
Zombie NIR TM Fixable Viability Kit	BioLegend	Cat# 423105
LEGEND plex mouse inflammation	BioLegend	Cat# 740446
panel with a V-bottom plate	G	
EnzyChrom TM Triglyceride Assay Kit	BioAssay Systems	Cat# ETGA-200
PicoSense Total Collagen Assay kit	BioMax	Cat# BM-COL-100
CORALL RNA-Seq V2 Library Prep Kit	Lexogen	Cat# 176.384
Poly(A) RNA Selection Kit	Lexogen	Cat# 157.96
QuantSeq 3' mRNA-Seq Library Prep Kit FWD	Lexogen	Cat# 191.24
Deposited data		
Mouse MASH RNA-seg transcriptomic data	In this study; Newly deposited in GEO	GSE279496
Mouse HSC RNA-seq transcriptomic data	In this study; Newly deposited in GEO	GSE279499
Human Liver gene expression data	GEO portal	GSE61260
Experimental models: Cell lines		
human LX-2 cells	Sigma-Aldrich	SCC064

(Continued on next page)



Continued				
REAGENT or RESOURCE	SOURCE	IDENTIFIER		
Experimental models: Organisms/strains				
C57BL/6 <i>Il-18bp</i> KO mice	Jang et al. ¹⁷	N/A		
C57BL/6 mice	Orient Bio	N/A		
Oligonucleotides				
Primes for mouse see Table S1	This paper	N/A		
Primes for human see Table S1	This paper	N/A		
Software and algorithms				
FlowJo 10.7.1	FlowJo	https://www.flowjo.com/solutions/flowjo		
ImageJ	U.S. Department of Health & Human	https://imagej.nih.gov/ij/download.html		
GSEA	Broad Institute	https://www.gsea-msigdb.org/		
GraphPad Prism8.0	GraphPad Software	https://www.graphpad.com/		
Other				
Captured Ezscope U200 microscope	Macrotech	N/A		
LSM880 Super Sensitive High Resolution	Carl Zeiss	N/A		
Confocal Laser Scanning Microscope				
TissueLyser II	Qiagen	N/A		
UV-Vis Nabi spectrophotometer	MicroDigital	N/A		
StepOnePlus real-time PCR system	Applied Biosystems	N/A		
Fuzion Solo 6X chemiluminescence system	Vilber	N/A		
SpectraMax plus 384 multiplate reader	Molecular Devices	N/A		
GentleMACS dissociator	Miltenyi Biotec	N/A		
FACS Lyric [™] machine	BD Biosciences	N/A		
Dri-chem NX500i hematology analyzers	Fuji	N/A		
ND-2000 Spectrophotometer	Thermo Fisher	N/A		
NovaSeq 6000	Illumina	N/A		
NextSeq 500/550	Illumina	N/A		

EXPERIMENTAL MODEL AND STUDY PARTICIPANT DETAILS

Study approval

Human study was conducted in accordance with principles of the Declaration of Helsinki and the Declaration of Istanbul. The study protocol, including the collection of blood samples, was approved by the Severance Hospital Institutional Review Board (IRB No. 4-2015-0184; 4-2020-0504). The animal experiments were approved and conducted in accordance with the ethical guidelines of the Kangwon National University Animal Care and Use Committee (KW-220412-6). STAM mice experiments were conducted at SMC Laboratories, Inc. (Tokyo, Japan); study number SLMN081-2209-2.

Human samples and group information

Human blood samples were obtained in accordance with relevant ethical regulations, and written informed consent was obtained from each participant. Before clinical sample collection, patients were informed, and their written consent was completed. Frozen liver tissues and blood plasma were obtained from Yonsei University Severance Hospital (Seoul, Korea). For healthy donors, individuals with no history of severe disease or medication were recruited and assessed through a questionnaire during the initial screening. Their medical history was re-evaluated three months later at the time of subsequent sampling. For MASH patients (NAS score \geq 4, Fibrosis stage \geq 2), severity of liver samples were assessed based on histologic NAS score with evidence of hepatic steatosis, ballooning, and inflammatory foci and the noninvasive nonalcoholic fatty liver disease and histologic fibrosis score. The inclusion criteria required participants to be over 19 years old with liver disease confirmed through histological, radiological, or laboratory testing. Exclusion criteria included individuals aged 18 or younger, those with a history of HCC diagnosis or treatment, or a history of transplantation. Each cohort consisted of 9 healthy controls and 23 MASH patients. Blood samples were obtained from healthy living donors for liver transplantation as well as patients diagnosed with MASH based on histologic diagnosis. The sectioned biopsy was performed in 2–3 mm piece of liver tissues. Human plasma and tissues were provided and analyzed using an ELISA (R&D Systems) kit according to the manufacturer's protocol.

Article



Animal experiments

Male 8-week-old C57BL/6J mice were purchased from Orient Bio Inc. (Gyeonggi-do, Korea), and IL-18BP KO mice were generated using the CRISPR/Cas9 system, as described previously. 17 8-week-old wild-type male mice or IL-18BP KO mice were fed for regular chow diet with tap water or FPC diet (TD.190142; Envigo, Indianapolis, IN, USA) with sugar water (fructose + glucose) for 15 weeks 8-week-old C57BL/6J wild-type or IL-18BP KO male mice were fed for chow or MCD (A02082002BR, Research Diets, New Brunswick, NJ) diet for 5 weeks ad libitum. For drug experiments, 8-week-old wild-type male mice were fed with FPC diet with sugar water for 19 weeks. APB-R3 (8 mg/kg, SAFA-hlL18BP; AprilBio Co., Ltd., Chuncheon, Korea), Liraglutide (100 mg/kg, Saxenda; Novo Nordisk, Bagsvaerd, Denmark), and APB-R3 + Liraglutide (Combined) were intraperitoneally injected to mice three times a week for 8 weeks because APB-R3 biologics is stably absorbed into systemic circulation through i.p. injection and the half-life of APB-R3 in mice was about 30 h¹⁷ 8 mg/kg dosage of APB-R3 was determined because this dosage didn't show any side effect with sufficient drug efficacy. For CCI₄ fibrosis model, C57BL/6J wild-type male mice were intraperitoneally injected with CCI₄ (Sigma-Aldrich, St. Louis, MO) dissolved in corn oil three times a week for 5 or 10 weeks, and APB-R3 and vehicle were administered three times a week. For induction of severe MASH model, C57BL/6J wild-type mice were fed for FPC diet with sugar water for 27 weeks. APB-R3 was intraperitoneally administered to mice for 8 weeks, and 5 mg/kg of MGL-3196 (Resmetirom; MedChemExpress, Monmouth Junction, NJ) was orally gavaged to mice daily for 8 weeks. For CDAA-HFD diet-induced MASH mice model, C57BL/6J wild-type male mice were fed for chow or CDAA-HFD (A06071302, Research Diets) diet for 13 weeks with tap water. After 6 weeks from start of experiment, CDAA-HFD-fed mice were intraperitoneally injected with APB-R3. For neutralization experiments, IgG2a matched as control antibody (10 mg/kg, BioXcell, West Lebanon, NH) and anti-IFN_γ (10 mg/kg, BioXCell) was injected during 5 weeks. In the T cell depletion experiment, anti-mouse CD4 (clone GK1.5, BioXcell) and anti-mouse CD8 antibody (clone 2.43, BioXcell) were administered intraperitoneally at a dosage of 300 mg/mouse to mice on an FPC diet for 17 weeks, followed by and additional injection of 50 mg/mouse three days later. The mice were sacrificed and analyzed 10 days post the initial injection. Rat IgG2b isotype control (BioXcell) antibody was used as control IgG antibody.

For induction of STAM model, 2-day-old male C57BL/6J mice were subcutaneously administered 200 mg streptozotocin solution and fed high-fat diet containing 57 kcal% of fat (HFD32, CLEA Japan, Tokyo, Japan). At 6 weeks of age, the drugs including APB-R3 or Telmisartan were administered to mice for 6 weeks. All mice were housed in cage under controlled conditions of temperature (22 \pm 2°C) and humidity (50 \pm 10%) on a 12 h light/12 h dark cycle schedule with free access to food and water. CO₂ euthanasia was performed, and liver or other tissues were fixed in 4% paraformaldehyde or stored frozen in liquid nitrogen. All experiments were performed in a blinded and randomized fashion.

Isolation and culture of hepatic stellate cells

Primary mouse liver cells were isolated from 8 to 10 weeks old male wild-type C57BL/6J mice (Jackson Laboratories) by perfusion of collagenase type IV (Sigma-Aldrich). The livers were perfused with 0.2 mg/mL of collagenase buffer in HBSS solution by injection of syringe toward the inferior vena cava as described previously.³⁷ To isolate HSCs, the nonparenchymal cell-containing supernatant was loaded onto 11.5% OptiPrep (Sigma-Aldrich) and centrifuged at 1,400 g for 15 min. After centrifugation, HSCs were collected at the pellet and cultured in Dulbecco's modified Eagle medium (DMEM) with 10% FBS and 1% penicillin/streptomycin for 4 days to spontaneously activate (D4 HSCs). The D4 HSCs were exposed to 150 mg/mL of APB-R3 (Aprilbio) overnight. The cells were cultured in an incubator with 5% CO₂ at 37°C. LX-2 cells (Merck Millipore, Darmstadt, Germany) were cultured in full medium of DMEM.

METHOD DETAILS

Glucose tolerance test

Glucose tolerance test was performed after a 12 h fast. Mice were intraperitoneally injected with 2 g glucose per kg of body weight (20% D-glucose (Sigma-Aldrich) in PBS). Glucose concentrations obtained from tail vein blood were measured subsequently at 0, 15, 30, 60, 120 and 180 min post-glucose administration using a Accu-chek blood glucose meter (Roche Diagnostics, Mannheim, Germany).

Staining of stellate cells and sectioned liver tissues

HSCs were washed with PBS and fixed with 2% cold methanol for 10 min at 4°C. The cells were then blocked with 5% bovine serum albumin (BSA; Sigma-Aldrich) for 1 h at room temperature and incubated overnight with the primary antibody (αSMA; Agilent DAKO, Santa Clara, CA). The secondary antibodies (Donkey anti-Mouse IgG Alexa Fluor 488; Thermo Fisher, Waltham, MA) were incubated at a 1:300 dilution for 1 h. Fluoro-Gel II with DAPI (Electron Microscopy Sciences, Hatfield, PA) was used to mount the cells. For paraffin-embedded, deparaffinization was carried out with xylene (Duksan, Ansan, Korea), followed by rehydration with 100%, 95%, and 70% ethanol. The sections were stained with hematoxylin and eosin (H&E; Sigma-Aldrich), Masson's Trichrome, or Picro-Sirius Red solution (Abcam, Cambridge, MA) according to the manufacturers' protocols. The prepared sections after antigen retrieval were stained with anti-type I Collagen (1:50; Southern Biotech, Birmingham, AL), anti-αSMA (1:50; Agilent DAKO) and anti-Desmin (1:50; Abcam). The secondary antibodies (Donkey anti-Mouse IgG Alexa Fluor 488, Donkey anti-Goat IgG Alexa Fluor 594 and Donkey anti-Rabbit IgG Alexa Fluor 647; Thermo Fisher) were incubated at a 1:300 dilution for 1 h. Cryo-sectioned frozen tissues were stained with heated Oil Red solution (Sigma-Aldrich) for 10 min. Stained sections were captured Ezscope U200 microscope



(Macrotech, Goyang, Korea) and LSM880 Super Sensitive High Resolution Confocal Laser Scanning Microscope (Carl Zeiss, Jena, Germany). The numbers of inflammatory foci were counted in each filed of X100 or ×200 magnified views by pathologists under blinded conditions. Stained areas in the sectioned tissues were measured by ImageJ software (NIH). Histological assessments were performed by pathologists under blind conditions. NAS and CRN fibrosis score was used. 38,39

Quantitative real-time PCR (gRT-PCR)

Liver tissue was homogenized using easy-BLUE (iNtRON, Seongnam, Korea) and TissueLyser II (Qiagen, Hilden, Germany). Total RNA was isolated using the RNeasy mini kit (Qiagen) following the manufacturer's protocol. After separating hepatocytes and HSCs, total RNA was isolated using RNeasy Micro kit (Qiagen). Concentration and quality of purified RNA were analyzed using a UV-Vis Nabi spectrophotometer (MicroDigital, Seoul, Korea), and reverse transcription of 0.04–1 mg RNA was performed. For cDNA generation, a high-capacity cDNA reverse transcription kit (Thermo Fisher) was used. The reaction of SYBR Green PCR master mix (Applied Biosystems, Foster City, CA), primers, and cDNA mixture was performed using StepOnePlus real-time PCR system (Applied Biosystems). The fold change of mRNA levels of the target gene was estimated by the equation $2^{-\Delta Ct}$ ($\Delta Ct = Ct$ of the target gene minus Ct of housekeeping genes such as 18S rRNA, *Gapdh*, or *Actb*). The fold change in gene transcription was shown based on a level of 1 in each control group. Used primer sequences are provided in Table S1.

Immunoblot

Total proteins from frozen liver tissue samples were extracted with RIPA buffer (ELPIS, Daejeon, Korea), and were separated with 10% sodium dodecyl sulfate-polyacrylamide gel electrophoresis (SDS-PAGE). Then, proteins were transferred to PVDF membranes. The membranes were blocked for 1 h at room temperature in Tris-buffered saline-Tween 20 (TBS-T) solution with 5% dry milk. After blocking, the membrane was incubated overnight at 4°C with mouse anti-αSMA (1:2000, Agilent DAKO), and rabbit anti-GAPDH (1:8000, BIOSS, Woburn, MA) antibodies. Membranes were afterward incubated for 2h at room temperature with goat anti-mouse secondary antibody (1:3000, Bio-rad, Hercules, USA) and goat anti-rabbit antibody (1:3000, Bio-rad). Subsequently, luminol enhancer solution and peroxide (iNtRON) was added to the membranes for 5 min. Proteins were visualized using a Fuzion Solo 6X chemiluminescence system (Vilber, Collegien, France).

Enzyme-linked immunosorbent assay (ELISA)

For ELISA experiments, frozen liver tissues were homogenized with protease inhibitors and RIPA lysis mixture buffer (Sigma-Aldrich) using a Tissue Lyser II (Qiagen). After centrifugation, supernatants were collected. Mouse blood was collected in EDTA tube and centrifuged at 4°C for 10 min to obtain plasma. ELISA kits to measure IL-18, IL-18BP, IFN_Y (R&D systems, Minneapolis, MN) and Pro-C3 (Novus Biologicals, Littleton, CO) were used according to the manufacturer's protocol. The calculation to measure free IL-18 levels was based on 1:1 binding ratio between IL-18 and IL-18BP with a dissociation constant (Kd) of 0.4 nM.¹⁴ Absorbance was measured at 450 nm by a SpectraMax plus 384 multiplate reader (Molecular Devices, San Jose, CA).

Flow cytometry

The liver tissues were homogenized in collagenase D (Sigma-Aldrich) buffer using a GentleMACS dissociator (Miltenyi Biotec, Auburn, CA). The homogenized tissues were centrifugated for 3 min at 500 rpm, and the obtained supernatant was centrifuged at 1700 rpm for 5 min to prepare non-parenchymal pellet. The non-parenchymal cells were obtained after stacking on 26% Percoll (GE Healthcare, Madison, WI) and centrifuging at 1700 rpm for 5 min. Hepatic immune cells were collected as pellets. Anti-CD16/32 (BioLegend, San Diego, CA) was added to block the Fc antibody receptor, washed, and cells were incubated with fluorescence-conjugated antibody containing BV786-anti-CD8 (BD Biosciences, Oxford, UK), PerCP/Cy5.5- or FITC-anti-Ly6C, FITC- or BV510-anti-CD45, APC/Cy7-anti-Ly6G, APC-anti-F4/80, PE/Cy7-anti-CD11b, FITC-anti-CD44, AF488-anti-NK1.1, AF647-anti-IL-18R, PerCP/Cy5.5-anti-CD4, PE-anti-CD49b, PerCP/Cy5.5-anti-B220, APC/Cy7-anti-CD49a, PE/Cy7-anti-CD3 and PE-anti-TIM4 (BioLegend) for 30 min. DAPI or zombie NIR (Biolegend) was used to exclude dead cells. To evaluate *ex vivo* responsiveness to IL-18 *ex vivo*, hepatic immune cells were stimulated with coated anti-CD3 antibody (1 mg/mL, BioLegend) and anti-CD28 antibody (2 mg/mL, BioLegend) in the presence or absence of recombinant murine IL-18 (20 ng/mL, PeproTech, Cranbury, NJ) for 4 h, followed by intracellular IFNγ staining with fluorescence-conjugated antibody e450-anti-FOXP3 (Thermo Fisher), PE or BV421-anti-IFNγ (Biolegend). FlowJo software (BD Biosciences) was used and analyzed on a FACS Lyric machine (BD Biosciences).

Plasma cytokine assay

The LEGEND plex mouse inflammation panel with a V-bottom plate (BioLegend) was used to compare cytokines in mouse plasma according to manufacturer's instructions. Briefly, frozen plasma samples were thawed and diluted 2-fold with assay buffer. Samples were placed to each well with capture beads and incubated at room temperature for 2 h on a plate shaker (800 rpm). Detection antibodies were added to each well after three times of washing the plate with wash buffer. The plate was incubated on a share for 1 h at room temperature. Streptavidin phycoerythrin (SA-PE) was added without washing and incubated on a shaker for 30 min at room temperature. Multiplex experiment was carried out using a FACS Lyric machine (BD Biosciences) after washing. Data were analyzed using FlowJo software (BD Biosciences).

Article



Measurement of hepatic triglycerides (TGs) and plasma biochemistry

For measurement of liver TG levels, frozen liver tissues were homogenized with RIPA lysis buffer using Tissue Lyser II (Qiagen). A lipid layer was obtained after centrifugation at 14,000 rpm for 10 min. TG was measured at 570 nm absorbance using a SpectraMax plus 384 multiplate reader (Molecular Devices) by the EnzyChrom Triglyceride Assay Kit (BioAssay Systems, Hayward, CA) according to the manufacturer's protocol. Mouse blood was collected in EDTA tube and then centrifuged at 6,000 rpm for 10 min at 4°C. The upper plasma was separated and obtained. Plasma ALT/AST or glucose levels were measured using Dri-chem NX500i hematology analyzers (Fujifilm, Tokyo, Japan).

Measurement of hepatic hydroxyproline

For hydroxyproline measurements, frozen liver tissue was homogenized with distilled water using a tissue Lyser II (Qiagen). Hydrochloride was added in the same amount and hydrolyzed by incubation at a 120°C heat block for 3 h. PicoSense Total Collagen Assay kit (BioMax, Daejeon, Korea) was used according to the manufacturer's protocol. Absorbance was measured at 560 nm.

RNA isolation for sequencing

Total RNA was isolated using Trizol reagent (Invitrogen). RNA quality was assessed by TapeStation4000 System (Agilent Technologies, Amstelveen, Netherlands), and RNA quantification was performed using ND-2000 Spectrophotometer (Thermo Fisher).

Library preparation and sequencing (mRNA-seq)

Libraries were prepared from total RNA using the CORALL RNA-Seq V2 Library Prep Kit (Lexogen, Inc., Vienna, Austria). The isolation of mRNA was performed using the Poly(A) RNA Selection Kit (Lexogen, Inc.). The isolated mRNAs were used for the cDNA synthesis and shearing, following manufacture's instruction. Indexing was performed using the Illumina indexes 1–12. The enrichment step was carried out using PCR. Subsequently, libraries were checked using the TapeStation HS D1000 Screen Tape (Agilent Technologies) to evaluate the mean fragment size. Quantification was performed using the library quantification kit using a StepOne Real-Time PCR System (Applied Biosystems). High-throughput sequencing was performed as paired-end 100 sequencing using NovaSeq 6000 (Illumina, San Diego, CA).

Library preparation and sequencing (QuantSeq)

For control and test RNAs, the construction of library was performed using QuantSeq 3' mRNA-Seq Library Prep Kit FWD (Lexogen, Inc.) according to the manufacturer's instructions. In brief, each total RNA was prepared and an oligo-dT primer containing an Illumina-compatible sequence at its 5' end was hybridized to the RNA and reverse transcription was performed. After degradation of the RNA template, second strand synthesis was initiated by a random primer containing an Illumina compatible linker sequence at its 5' end. The double-stranded library was purified by using magnetic beads to remove all reaction components. The library was amplified to add the complete adapter sequences required for cluster generation. The finished library is purified from PCR components. High-throughput sequencing was performed as single-end 75bp sequencing using NextSeq 500/550 (Illumina, San Diego, CA).

Data analysis for RNA-seq

A quality control of raw sequencing data was performed using FastQC. Sequenced reads were trimmed for adapter sequences and low-quality filtered using BBDuk. Then the clean reads were mapped to the reference genome using STAR. The quantification of reads was processed using HTSeq-count. The Read Counts were processed based on TMM+CPM normalization method using using Python "conorm" package. Gene ontology was identified by DAVID functional annotation tool (NIH) and Gene Set Enrichment Analysis (GSEA) tool. Heatmap of broad gene expressions was generated by phantasus package (https://artyomovlab.wustl.edu/phantasus/). Data mining and graphic visualization were performed using ExDEGA (Ebiogen Inc., Seoul, Korea). The transcriptomic sequencing results have been deposited in the Gene Expression Omnibus (GEO) database with the accession number: GSE279496 and GSE279499.

QUANTIFICATION AND STATISTICAL ANALYSIS

All values are represented as the means \pm SEM. Statistical analyses were conducted using an unpaired two-sided Student's t test for simple comparisons or a one-way ANOVA with Tukey's post hoc test for multiple comparisons. p < 0.05 was considered significantly different. The analysis was conducted by Graphpad Prism 8.0 (GraphPad Software Inc., San Diego, CA).